NASA CR-72613
HTL TR NO. 92

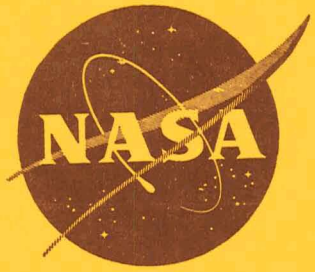

INTERACTION OF A HEATED JET WITH A DEFLECTING STREAM

J. W. Ramsey
R. J. Goldstein

prepared for

NATIONAL AERONAUTICS AND SPACE ADMINISTRATION

NASA CONTRACT NO. NAS 3-7904

HEAT TRANSFER LABORATORY

MECHANICAL ENGINEERING DEPARTMENT

UNIVERSITY OF MINNESOTA

NASA CR-72613
HTL TR NO. 92

SUMMARY REPORT

INTERACTION OF A HEATED JET WITH A DEFLECTING STREAM

by

J. W. Ramsey and R. J. Goldstein

prepared for

NATIONAL AERONAUTICS AND SPACE ADMINISTRATION

April 1970

CONTRACT NAS 3-7904
TECHNICAL MANAGEMENT
NASA Lewis Research Center
Cleveland, Ohio
Lewis Project Manager; Francis S. Stepka

University of Minnesota
Institute of Technology
Department of Mechanical Engineering
Minneapolis, Minnesota 55455

ABSTRACT

An experimental investigation of the interaction of a heated jet with a deflecting flow has been performed in a wind tunnel. The secondary (jet) flow is introduced at angles of 90^{o} and 35^{o} to the mainstream flow direction. Visualization studies using tufts of yarn and a carbon dioxide-water fog are reported. Temperature profiles in the interaction region are presented for blowing rates (ratio of mass flux of injected gas to mass flux of freestream) from 0.1 to 2.0 for normal injection and at blowing rates of 1.0 and 2.0 for 35 degree injection. Velocity and turbulence intensity profiles are reported for normal injection at blowing rates of 1.0 and 2.0.

NOMENCLATURE

D	diameter of injection tube
M	blowing rate parameter, $M = \rho_2 U_2 / \rho_\infty U_\infty$
T	temperature
T_2	temperature of secondary injected air
T_∞	mainstream temperature
U	velocity
U_2	average air velocity in injection tube
U_∞	mainstream velocity
$\overline{U}$	time average velocity
u_1	fluctuating component of velocity in the direction of $\overline{U}$
$\overline{u_1^2}$	time average value of the square of the velocity u_1
X	distance downstream of injection hole, see Figure 1
Y_J	vertical position of maximum velocity at $Z = 0$
Y	distance normal to tunnel floor, referenced to injection hole, see Figure 1
Z	lateral distance from injection hole, see Figure 1
β	angle between the direction of injection and the direction of the mainstream in the X-Y plane
θ	temperature difference; $\theta = T - T_\infty$
θ_2	temperature difference; $\theta_2 = T_2 - T_\infty$
θ_{aw}	adiabatic wall temperature minus mainstream temperature
θ_{max}	maximum θ for a given temperature profile
θ_w	the value of θ at the wall

ρ density

ρ_2 density of secondary air

ρ_∞ density of mainstream

INTERACTION OF A HEATED JET WITH A DEFLECTING STREAM

by

J. W. Ramsey and R. J. Goldstein
University of Minnesota

I. SUMMARY

This report summarizes an experimental investigation of the interaction of a heated subsonic circular air jet issuing into a subsonic main flow of air.

Visualization studies present information on the general shape and path of the jet. The instantaneous jet boundary is found to be very irregular with large scale eddies. As the jet enters, mainstream air is entrained from the sides filling the low pressure region immediately downstream of the jet. At large blowing rates a reverse flow region is found to exist on the downstream side of the entering jet.

Temperature profiles show increasing jet penetration with increasing blowing rates. The wall temperature is influenced in two counteracting ways as the blowing rate is increased. The increased secondary mass flow and resulting increased enthalpy addition to the stream tends to increase the temperature. However, the increased penetration moves the jet axis farther from the wall and tends to lower the wall temperature.

Comparisons between perpendicular and 35 degree injection show that there is less penetration and less vertical and lateral spreading for 35 degree injection.

Velocity profiles for a jet entering perpendicular to the mainstream are presented. Low velocities are measured near the wall directly downstream of the incoming jet. Above this region the velocity increases reaching a maximum which can be greater than the freestream velocity and then decreases to the freestream value. Very large turbulence intensities are measured in the low velocity region. Some distortion of the mainstream is observed as far as twenty-six diameters downstream of the injection position.

II. INTRODUCTION

The interaction of a circular jet with a subsonic deflecting stream has recently been the subject of renewed interest. This type of flow configuration exhibits many features such as production of large scale eddies and high levels of turbulence including flow reversal which are of interest in basic fluid dynamics. In addition, there are a number of applications of this type of flow, such as film cooling, mixing of two fluid streams, and impingement cooling. It is of interest to note that these different applications have different desideratums in terms of the path of the jet. Thus, in film cooling it is of interest that the jet remains as close as possible to the wall from which it issues. In mixing of two streams it is usually desirable that the jet mixes fully and uniformly with the main flow. With impingement cooling the jet should penetrate across the flow and spread itself out on the surface opposite that from which it is injected.

The present paper reports on the experimental results of an investigation which is concerned with film cooling utilizing injection of air through circular holes into an air mainstream. The overall aim is to obtain a better understanding of film cooling.

In order to accomplish this it is necessary to study the more fundamental process by which fluid jets interact with mainstreams in the neighborhood of solid surfaces. With further understanding of the basic processes the ability to predict film cooling as well as the other applications mentioned above should be greatly enhanced.

The study reported herein concerns primarily the interaction of a jet with the flow stream. Results are reported of flow visualization studies, temperature measurements in the flow field for heated injection, and velocity measurements in the flow field for an unheated jet. A turbulent boundary layer exists on the wall through which the jet exits, and this wall is designed to be adiabatic. Temperature profiles are reported for blowing rate parameters from 0.1 to 2.0 for normal injection, and blowing rate parameters of 1.0 and 2.0 for 35^{o} injection. Velocity and turbulence intensity profiles are obtained at blowing rate parameters of 1.0 and 2.0 for injection of an unheated jet perpendicular to the mainstream.

III. REVIEW OF PREVIOUS STUDIES

The flow field following injection from a single hole into a mainstream has received considerable attention. Lee (1)* presents a brief review of the literature. A qualitative description of the interactions which occur and the shape of the flow field is presented by Keffer and Baines (2) and Abramovich (3). A flow diagram for a secondary flow entering through a circular tube normal to the free-stream is presented in Figure 1, based on the discussions in (2) and (3) and on flow visualization results of the present study. As the jet of fluid leaves the surface it retards the main flow along the upstream side of the jet causing an increased pressure. At the downstream side of the jet a rarefaction occurs. This pressure difference provides the force necessary to deform the jet. Jordinson (4) has compared this flow to that around a porous cylinder with suction. The jet takes on a "horseshoe" or "kidney" shape. Abramovich (3) explains this deformation of the jet's cross-section by the character of its interaction with the deflecting flow. Because of the intensive intermixing of the jet with the deflecting flow, a turbulent layer quickly develops around the periphery of the jet. The slower peripheral particles of the jet are more forcefully bent away from the initial direction than the higher velocity particles of the core and are moved along more curved trajectories by the deflecting flow leading to the horseshoe shape. The deflecting flow and circulatory zones cause the particles of the jet to branch

---

* Underlined numbers in parentheses designate references listed in the Bibliography.

out more and more from the plane of symmetry. Consequently, the legs of the "horseshoe" move apart. This gives rise to additional circulatory or vortex motion in the jet. The action of the vortices augments the entrainment of fluid, causing internal circulation and large scale mixing within the jet.

The deformation and turning of the jet is strongly affected by the mass velocity ratio or blowing rate, M. In general, the larger the blowing rate the farther the injected fluid penetrates into the main flow. With normal injection at blowing rates up to approximately 4 the potential core of the jet (the region where the velocity is equal to the initial jet velocity) is deflected by the pressure field (2). At still larger blowing rates the potential core is conical with the apex almost directly above the center of the jet orifice.

Experimental studies to determine the flow conditions with isothermal mixing of a jet and mainstream of the same fluid are described by a number of investigators (1, 2, 3, 4, 5). In these investigations the fluid jet is injected normal to the mainstream and at blowing rates greater than or equal to two. Gordier (5) used water while in the other investigations air was used. The general shape of the deflected jet axis is essentially the same in the various investigations (6). The measured height of the jet axis using air as the working fluid agrees with an empirical equation within approximately ten percent in air tests (2, 4), while the jet is about 20% higher in a study in which water was used (5). The greater penetration in the water experiments may be due to the relatively thick mainstream boundary layer which was present.

One semi-empirical analysis (3) for the position of the jet axis in a deflecting flow consists of a force balance on the jet using measured jet cross-sections and expansion rates and an empirical aerodynamic force constant. Proper selection of empirical constants yields reasonable agreement with experimental data for a distance of approximately three or four diameters from the point of injection. The distortion and deflection of a normal jet due to dynamic pressure forces acting on it during the first diameter of travel has also been calculated (7). Potential flow is assumed and the pressure distribution about the jet at the plane of egress is assumed identical to that about an infinite cylinder of the same diameter in an air stream at the same Reynolds number. The path of the jet axis is then determined by extrapolating the deflection curve. Fair agreement is indicated (7) with experiment for approximately three diameters downstream of the injection location.

Extensive studies of the penetration of heated air jets into deflecting air streams have been conducted by NACA. The jets are introduced at considerably higher temperatures than the main flow (160 to 185°C), and the depth of penetration is sensed with a temperature probe. The first investigation (8) reports the penetration of a circular air jet directed perpendicular to the deflecting flow. The penetrating depth of the upper edge of the jet, defined as the height above the wall at which the temperature of the jet exceeds the temperature of the mainstream by about ½°C, is empirically correlated as a function of density and velocity ratios of the jet and mainstream flows. The correlation is improved by the inclusion of the orifice

coefficient (9) in defining an effective orifice diameter (10). Studies of depth penetration from circular, square and elliptical orifices (10) indicate the penetration depth is greatest for square orifices and lowest for circular orifices. Gordier (5) compares his results for the location of the upper edge of the jet, as determined from visualization studies, with the results of (10) and finds good agreement. Temperature profiles are measured for perpendicular injection (11) and for angles of 90^{o}, 60^{o}, 45^{o} and 30^{o} to the main flow (12). The tunnel used for the NACA experiments is quite narrow and most of the data is taken at downstream positions where the jet has expanded to the side walls. This confinement of the jet by the side walls may strongly effect the shape of the measured profiles and the penetration depth.

An experimental investigation has been carried out at the University of Minnesota to determine adiabatic wall temperature distributions with injection of air through a discrete circular hole into a turbulent boundary layer of air on a flat plate (13, 14). These experiments are conducted for a range of blowing rate parameters from 0.1 to 2.0 with an air jet entering at an angle of either 35^{o} or 90^{o} to the main flow. Basic trends for the two injection angles are found to be similar with differences occuring only at large injection rates. The dimensionless adiabatic wall temperature or effectiveness (θ_{aw}/θ_2) reaches a maximum for a blowing rate parameter of approximately one half. Injection at an angle of 35^{o} yields considerably higher film cooling effectiveness, especially at larger blowing rates.

IV. APPARATUS AND OPERATING CONDITIONS

Wind Tunnel

The present investigation is carried out in a subsonic wind tunnel capable of air velocities of up to seventy meters per second in the test section. The main flow of air, drawn from the room, passes through an entrance section, test section, and diffuser. It then flows to the blower, from which it is discharged through a silencer to the outside. The tunnel is described in detail in References (6, 13, and 14).

The test section of the wind tunnel is 20.3 cm x 20.3 cm in cross section. The mainstream turbulence intensity in the absence of secondary flow is approximately 0.5 percent at a mainstream velocity of 30 meters per second. A 0.064 cm diameter boundary layer trip wire is located on the bottom wall of this segment approximately 3.8cm downstream from the end of the contraction section. The downstream end of the injection tube is about 20cm from this trip with the normal injection tube and about 45 cm for the 35^{o} tube. The injection of the secondary air is through a 2.35cm ID stainless steel tube approximately one meter long. Fully developed turbulent flow is present at the tube exit. The secondary air temperature, T_2, is taken as that measured by thermocouples attached to the injection tube at positions 4½ and 6 diameters upstream of its end (both of which indicate the same temperature).

The test section downstream of the injection location contains thermocouples for measuring wall temperature distribution downstream of the injection. The bottom wall is an adiabatic test plate designed

according to the following considerations: it should have a rapid thermal response and it should be adiabatic including low conduction in all directions parallel to the plate surface. It consists of a 0.32 cm Textolite plate thinned to 0.16cm at the thermocouple locations, backed by approximately 5 cm of Styrofoam insulation.

Probes

The temperature probe to survey the air stream consists of a thermocouple stretched across two supports. The junction is made large (0.13 cm diameter or approximately ten wire diameters) in order to minimize conduction effects in the three dimensional temperature field investigated. The reference junction for the probe is located on the wall of the tunnel test section at a point upstream of the injection which is at mainstream temperature and not affected by the secondary flow, so that the probe indicates the temperature difference between the large junction and the mainstream. A traversing assembly for the probe provides movement in the axial direction and in the direction normal to the adiabatic test plate. The lateral position of the probe, relative to the injection location, is varied by moving the injection section of the tunnel.

A hot film probe with a 0.025 mm diameter x 0.51 mm long sensor is used for velocity measurements. The probe is operated by a constant temperature hot wire anemometer system which, in addition to maintaining the sensor at constant temperature, provides a signal monitoring voltmeter. The probe is calibrated in the tunnel in the absence of secondary flow by measuring the freestream velocity using a total pressure probe as reference. The turbulence intensity in the flow

field is also measured using the hot film probe anemometer.

Tunnel Operating Conditions

The tunnel operating conditions are basically the same as those used earlier (13). These are : 1) a fully developed turbulent boundary layer on the test surface in the absence of secondary flow, 2) mainstream velocity of either 30 or 61 meters per second, 3) boundary layer displacement thickness at the 90^{o} injection location of 0.09 cm and 0.07 cm for 30 and 61 meters per second respectively and at the 35^{o} injection location of 0.14 cm and 0.12 cm for 30 and 61 meters per second respectively, 4) fully developed turbulent pipe flow at the end of the injection tube in the absence of primary flow, 5) a uniform temperature distribution at the end of the injection tube in the absence of primary flow, 6) injection air temperature approximately $55^{o}C$ higher than that of the mainstream for temperature studies, 7) injection temperature approximately equal to that of the mainstream for velocity studies and 8) steady state conditions during the tests.

The probe is positioned along the tunnel centerline and the various lateral positions are obtained by translating the injection tube laterally relative to the tunnel centerline. The distributions are laterally symmetric, and usually the tube is only moved in one direction from the tunnel centerline.

V. EXPERIMENTAL RESULTS

Visualization Studies

1. Tuft Study

A small tuft of yarn attached to the end of a thin rod was used to examine the flow field in and around the jet. A sketch of the observed field is shown in Figure 1. As the jet enters it leaves a void (low pressure condition) downstream of it which is filled by mainstream air moving around the jet. In the region near the wall and for a distance almost halfway around the jet the flow patterns look similar to what is found around a cylinder in cross flow. The flow continues around the jet and into the apparent low pressure region on its downstream side.

At a blowing rate of two, immediately downstream of the injection location the incoming mainstream air moves parallel to the floor of the tunnel and laterally with almost no component of velocity in the downstream direction. As the mainstream air moves towards the zero lateral position (Z/D=0) it begins to move upward away from the wall, apparently being entrained by the jet. This region where the air enters in from the side and then moves vertically extends approximately two diameters downstream and is a region of extreme fluctuations.

Approximately one diameter downstream, as the air moves vertically away from the wall it reaches a height where it turns upstream and reverse flow exists. At greater distances from the wall the flow changes from reverse to forward flow. The inclination of the jet relative to the mainstream direction

reaches zero between 2½ and 3 diameters from the wall.

Farther downstream the flow, after rising from the wall, turns downstream rather than upstream and lateral components away from the centerline are also observed, indicating the possible formation of vortices as suggested by previous investigators (2, 3). It is not possible to follow this circulation pattern away from the centerline with the tuft since the outer portion of the vortex flow becomes overwhelmed by the main flow and the lateral velocities appear to diminish rapidly. At distances greater than two diameters downstream the lateral velocity components diminish with axial distance until at approximately ten diameters no lateral velocity is observable.

Tufts were also used at a second blowing rate, M = 1. The trends observed were the same as those for the higher injection rate, the mainstream flow being drawn in to fill the void on the downstream side of the jet, this flow moving inward and then upward. Finally, depending on the axial position, the flow moves either upstream (reverse flow) or downstream and is then entrained by the jet. The principle difference between the flow patterns of the two blowing rates is that at the lower injection rate the vertical components of velocity in all regions are smaller.

Table 1 shows the inclination of the flow in the X-Y plane as determined from the tufts.

Table 1 Angle of Inclination to the Mainstream in the X-Y Plane (degrees) Measured with Tuft, Z/D = 0

	M = 2			M = 1		
Y/D	X/D=3	X/D=5	X/D=10	X/D=3	X/D=5	X/D=10
1/4	0	0	0	0	0	4
1/2	5	0	0	7	0	3
3/4	20	5	0	4	2	0
1	30	15	5	0	0	
1-1/4	45	15	5			
1-1/2	30	20	5			
1-3/4	25	10	5			
2	20	10	5			
2-1/4	15	10	5			
2-1/2	10	10	5			
2-3/4	5	5	5			
3	0	0	0			

2. Photographic Study

In order to observe the jet as it interacts with the mainstream, a carbon dioxide-water fog is injected through the injection tube. The fog is produced by putting solid carbon dioxide and hot water in a container fitted with a tube to allow passage of the resulting fog to the injection tube and into the tunnel. The mass flow rate is determined from the change in weight of the dry ice-water container. A blowing rate of unity was achieved by operating the tunnel with a mainstream velocity of fifteen meters per second. White marking

tapes (see Figure 2) are placed axially down the centerline (i.e., at Z/D=0), partway across the span at X/D=1, and spanning the full width of the tunnel at X/D=5 and X/D=10.

Figures 2a and 2b, taken from above the jet, show the lateral spreading of the jet to be quite limited. Figures 2c and 2d, taken from the side and downstream of the incoming jet show the penetration and turning of the jet. Note that at shorter exposure time, 1/1000 sec., the jet is irregularly shaped and intermittent, indicating large scale eddies. To ensure that the intermittancy pictured is due to the interaction between the jet and mainstream and is not introduced by irregularities in the secondary flow system, the top of the tunnel was removed and pictures taken at 1/1000 sec. of the jet in still air. These pictures indicate no irregularities in the jet flow.

Temperature Distribution

Temperature profiles are presented in terms of the dimensionless temperature ratio θ/θ_2 for injection normal to the mainstream at blowing rates of M = 0.1,0.5, 1.0, and 2.0. A mainstream velocity of 61 meters per second is used for M = 0.1 and 30 meters per second for the other blowing rates. Check runs made for M = 0.5 at a mainstream velocity of 61 meters per second were found to have temperature profiles similar to those obtained at 30 meters per second. Temperature profiles are also obtained for two blowing rates (1.0 and 2.0) with injection at

an angle of 35 degrees to the main flow direction. The mainstream velocity for these tests is 30 meters per second.

The temperature profiles at Z/D=0 for normal injection are presented in Figure 3. At M = 0.1, the lowest blowing rate investigated, little or no penetration of the secondary air into the mainstream occurs. The maximum temperature occurs near or at the wall. As the jet moves downstream it spreads and the maximum temperature decreases.

At a blowing rate of 0.5 the jet penetrates significantly into the main flow. At X/D=1.37 the maximum temperature occurs at a position 0.6 diameters above the wall. In addition to the increased penetration, the wall and maximum temperatures also increase in going from M = 0.1 to M = 0.5. As the jet travels downstream it spreads in such a way that the location of maximum temperature moves closer to the wall.

The profiles for the higher blowing rates, M = 1.0 and 2.0, indicate larger penetrations with increasing blowing rate. Note that for M = 1.0 the position of maximum temperature remains nearly constant in going from X/D = 1.37 to X/D = 3.06. Beyond X/D = 3.06 the location of the maximum temperature decreases somethat with increasing axial distance as before. This is consistent with the previously described visualization study in which the use of tufts indicated that the jet is still moving slightly away from the wall at X/D = 3 and is essentially turned in the direction of the mainstream at X/D = 5. At the largest blowing rate investigated, M = 2.0, the jet penetrates sufficiently far into the main flow that the wall temperature is nearly unaffected by its presence. The position

above the wall of the maximum temperature is found to increase with increasing axial distance for the entire range considered, consistent with the tuft measurements.

The temperature profiles measured at a lateral position one diameter from the jet axis are presented in Figure 4. Notice that for M = 0.1, the maximum temperature increases with axial distance, due to the increasing lateral width of the jet as it moves downstream. Comparing the profiles for the various blowing rates at Z/D = 1.0 shows that the lateral spreading of the jet increases with blowing rate.

The spreading effects can be better observed by presenting the data in the form of lines of constant dimensionless temperature, θ/θ_2, at a given axial plane normal to the tunnel floor. A number of these constant temperature contours are presented in Figures 5 through 8.

At a blowing rate of M = 0.1, Figure 5, the constant temperature contours indicate smooth or regular spreading in both the vertical and lateral directions. Figure 6 shows the effect of penetration of the jet for M=0.5. At axial distances of 1.37 and 3.06 diameters downstream the highest temperature regions are seen to be in the air stream above the wall. At the position X/D=1.37 the jet appears to be starting to develop the characteristic kidney shape observed in previous velocity studies at higher blowing rates, (2, 3, 4, 5). Figure 7 shows a more pronounced kidney shape at X/D=1.37 for M=1.0. As the jet moves downstream it spreads in such a way that the constant temperature lines become nearly circular. Increasing the blowing rate to M=2.0, Figure 8, results in the jet penetrating sufficiently

that it is almost totally above the wall. The contours indicate that the temperature of the air flowing next to the wall is only slightly affected by the jet. This air is very likely mainstream air which has moved around and under the jet.

The constant temperature contours also depict the effect of secondary injection on the adiabatic wall temperature distribution. At low injection rates the maximum temperature occurs on the wall and along the centerline. The limited amount of heated mass injected results in this maximum temperature being relatively low and causes it to decrease rapidly with increasing axial distance. Increasing the amount of injected air raises the wall temperature until a point is reached (approximately M = 0.5) where the increased penetration causes the jet to move away from the wall. The wall temperature then decreases with increasing injection rate. An injection rate is reached where the jet is totally above the wall and the wall temperature is close to the mainstream temperature. For injection normal to the mainstream this occurs at approximately M = 2.

Some temperature profiles for a round jet directed normal to the mainstream have been measured previously (11, 12). One of the profiles in each of the reports is for a blowing rate and axial position similar to one considered in the present study. A comparison, (6), indicates reasonable agreement which is somewhat surprising since in the earlier investigation the jet is confined by the tunnel walls.

A limited number of temperature profiles for injection at an angle of 35 degrees to the mainstream direction are presented in Figure 9. (Additional figures representing temperature distributions

at various positions and blowing rates are shown in the appendix for injection at 90^{o} and 35^{o}.) At a blowing rate of M = 1 the jet penetrates well into the mainstream. At the zero lateral position the penetration depth, as characterized by the position of maximum temperature, is seen to increase with increasing axial distance. For normal injection at M = 1.0 recall that the vertical height of maximum temperature decreased with increasing axial distance for X/D greater than approximately three. The depth of penetration is less for 35^{o} injection. For perpendicular injection the maximum temperature at X/D = 1.37 and Z/D = 0 occurs at Y/D = 1.2 while for 35 degree injection the maximum jet temperature has not penetrated to that depth as far downstream as X/D = 9.8.

Away from the axis the temperature level decreases rapidly when going from Z/D = 0.5 to Z/D = 0.75. The jet does not spread to Z/D = 1 until approximately X/D = 9.8. This spreading is considerably less than that observed for normal injection (cf. Figure 8).

A significant effect of reduced penetration as compared to normal injection is a much slower decline of the maximum temperature with axial distance for injection at 35^{o}. Approximately ten diameters downstream and at Z/D = 0 the maximum dimensionless temperature, θ/θ_2, is 0.5 for thirty-five degree injection and 0.2 for perpendicular injection, both for M = 1.0.

The same comparisons between the results for the two injection angles that are made for M = 1.0 can be made for M = 2.0. Specifically, for 35 degree injection the penetration depth is less, and the temperature drops less rapidly in the axial direction, but more rapidly in the lateral direction.

The jet penetration as a function of axial position is shown in Figure 10 for blowing rates of M=2.0 and 1.5 with normal injection and a blowing rate of M=2.0 with 35^{o} injection. The measured positions of maximum velocity (to be discussed later) are also included. An empirical relation for determining the axis from the position of maximum velocity of a circular jet deflected by an external flow is presented by Abramovich (3). The relation is:

$$\frac{X}{D} + 0.5 = \frac{\rho_\infty U_\infty^{\,2}}{\rho_2 U_2^{\,2}} \left(\frac{Y_J}{D}\right)^{2.55} + \frac{Y_J}{D}\left[1 + \frac{\rho_\infty U_\infty^{\,2}}{\rho_2 U_2^{\,2}}\right] \cot \beta \qquad (1)$$

The experiments from which this equation was derived were carried out for $45^{o} \leq \beta \leq 90^{o}$ and $2 \leq \frac{\rho_2 U_2^{\,2}}{\rho_\infty U_\infty^{\,2}} \leq 22$ or assuming $\rho_2 = \rho_\infty$ $1.4 \leq M \leq 4.5$. The jet penetration predicted by equation 1 is included in Figure 10. The figure shows that the velocity data of the present investigation for M > 1.5 is in good agreement with Abramovich's empirical prediction. The largest difference, at X/D = 10, is less than ten percent. The position of maximum temperature is below the position of maximum velocity.

Velocity Distributions

Velocity distributions are measured for an unheated jet at two blowing rates, M = 1.0 and 2.0, for a mainstream velocity of 30 meters per second. The cylindrical probe sensor is aligned with its axis parallel to the Z axis so that the velocity measured is in the X-Y plane. The direction of the velocity in this plane is not described by the probe measurements. Therefore what are actually measured with the probe are velocity magnitudes in the X-Y plane.

These values along with the tuft studies give a picture of the velocity field.

In addition to the mean velocity, the velocity fluctuations u_1 in the X-Y plane are also measured in terms of the turbulence intensity, $(\sqrt{\overline{u_1^2}})/\bar{U}$. In converting voltage output readings of the constant temperature anemometer to mean velocity and turbulence intensity values the assumption is made that the fluctuating components of velocity are small relative to the mean velocity. At a turbulence intensity of 0.5 approximately ten percent error (in intensity) can be introduced by the assumption of low turbulence while this error drops to 2.5 percent for a turbulence intensity of 0.25 (6). The error in velocity introduced by the assumption of low turbulence is approximately six percent for a turbulence intensity of 0.5 dropping to 1.5% for a turbulence intensity of 0.25 (6). The maximum turbulence intensity observed in this investigation is approximately 0.6. In addition to errors introduced by turbulence, reading errors of 10% and 2% are estimated to exist in the turbulence and velocity measurements respectively.

The velocity and turbulence distributions for the blowing rate of M = 1.0 and the lateral position Z/D = 0 are presented in Figure 11. Also included in the figure are lines indicating the positions of maximum temperature as measured in the temperature study. To further indicate how the temperature distribution compares with the velocity, the position at which $\theta/\theta_2 = 0.1$ is indicated. At axial positions where the flow angle of inclination to the mainstream in the X-Y plane is available from the tuft study this information is

tabulated on the figures. For X/D = 1.37 there is a region of nearly constant low velocity from the wall to an elevation of approximately Y/D = 1. In this region, while the magnitude of the velocity is nearly uniform, the visualization study using tufts indicates the flow direction is very nonuniform. Included in this region is some reverse flow. It is into this region, particularly near the wall, that the tuft studies indicate a sizeable mass flow from the mainstream. As might be expected from the nature of the flow, the turbulence level in this region is very large. Above this region the velocity increases until a maximum is reached at approximately 1.5 diameters above the wall. At this point the velocity is in the the direction of the main flow. The position of maximum velocity is seen to be above that of the temperature as indicated earlier in Figure 10. Farther from the wall the velocity decreases until it equals that of the mainstream.

As the jet moves farther downstream it is turned and accelerated in the direction of mainstream flow. This acceleration appears to take place both along the upper and lower edge of the jet, as indicated by the velocity peak near the wall. As the velocity increases, the turbulence level drops. The results of the tuft study, tabulated on the figure, indicate that the jet flow is nearly in the direction of the mainstream for axial distances greater than three diameters. A slight distortion of the velocity field still exists far downstream. This is apparent in Figure 11 at an axial position of X/D = 26.24 where the profile for M = 0, also measured with the hot film probe, is compared with that for M = 1.0.

Velocity and turbulence profiles are presented for a blowing rate of M = 2.0 in Figure 12. (Additional data on the velocity distributions are contained in the appendix.) These profiles are similar in shape to those for M = 1.0. As expected, increasing the blowing rate increases the height above the wall at which the maximum velocity occurs. Note also the region of reverse flow at X/D = 1.37.

Coupled with the increased penetration at the higher blowing rates is the slower turning of the jet into the direction of the main flow as indicated by the flow directions measured with the tuft. These results are tabulated on Figure 12 for easy reference.

VI. RESUME

The interaction of a heated subsonic circular air jet issuing into a subsonic mainflow of air has been investigated experimentally. The jet is introduced into the test section through a circular tube, whose exit is flush with a well-insulated wall of the test tunnel. In the absence of a secondary flow, a fully developed flat plate turbulent boundary layer is present and the freestream turbulence intensity is approximately 0.5 percent.

Visualization studies present information on the general shape and path of the incoming jet and indicate that upon entry to a deflecting flow the jet boundary is very irregular with large scale eddies.

As the jet enters, mainstream air is drawn in from the sides to fill the low pressure region immediately downstream of the jet. At large blowing rates a reverse flow region exists on the downstream side of the entering jet.

Temperature profiles for injection perpendicular to the mainstream show the jet penetration increases with increasing blowing rate parameter. The maximum temperature occurs at or near the wall for M=0.1 while for M=2.0 the maximum is at a height greater than two diameters above the wall even quite close to the jet entrance.

Increasing the blowing rate parameter influences the wall temperature in two counteracting ways. The increased secondary mass flow and resulting increased enthalpy addition to the stream tend to increase the temperature while the increased penetration moves the path of the jet's maximum temperature farther from the wall and tends to lower the wall temperature. The first effect predominates at the lower blowing rates (M 0.5). At larger blowing rates the effect of increased penetration causes the wall temperature to decline with increasing blowing rate. At M=2.0 the jet penetration is such that the jet has very little effect on the wall temperature.

Injection at an angle of thirty-five degrees to the direction of main flow exhibits less penetration and less spreading in both the vertical and lateral directions than perpendicular injection. The reduced spreading in the vertical direction occurs at both the top and bottom of the jet. The reduced spreading along the bottom of the jet results in less effect of the jet on the off-axis wall temperature.

In an unheated jet entering perpendicular to the mainstream

low velocities are measured directly downstream of the incoming jet. Above this region the velocity increases reaching a maximum greater than the freestream velocity and then declines to the freestream value. The turbulence intensity is found to be very large in the low velocity region. As the jet moves farther downstream the low velocity region is accelerated by the mainstream and the turbulence level drops. Some distortion of the velocity profile, as compared to the no-blowing condition, exists as far as 26 diameters downstream of the injection position.

A comparison of the velocity and temperature studies shows the position of maximum velocity to be somewhat farther from the wall than the position of maximum temperature for the same blowing rate parameter. This, coupled with the tuft study, suggests the air in the region of maximum velocity is in the outer region of the jet which is accelerated more than the region near the wall.

VII. BIBLIOGRAPHY

(1) C. C. Lee, "A Review of Research on the Interaction of a Jet with an External Stream," Brown Engineering Co., Inc., Huntsville, Ala. Research Labs., Rep. No. TN-R-184, March 1966. (Defense Documentation Center acquisition number AD 630 294).

(2) J. F. Keffer and W. D. Baines, "The Round Turbulent Jet in a Cross Wind," J. Fluid Mech., 15, 4, 481-497 (1963).

(3) G. N. Abramovich, The Theory of Turbulent Jets, M.I.T. Press, Massachusetts Institute of Technology, Cambridge, Massachusetts, 541-556 (1963).

(4) R. Jordinson, "Flow in a Jet Directed Normal to the Wind," Aero. Res. Council, R & M, No. 3074 (1956).

(5) R. L. Gordier, "Studies on Fluid Jets Discharging Normally into Moving Liquid," St. Anthony Falls Hyd. Lab., University of Minnesota, Tech. Paper, No. 28, Series B (1959).

(6) J. W. Ramsey, "The Interaction of a Heated Air Jet with a Deflecting Flow," Ph.D. Thesis, University of Minnesota (1969).

(7) J. P. Fraser, "Three-Dimensional Study of a Jet Penetrating a Stream at Right Angles," Journal of the Aero. Sciences, 21, 1, 59-61 (1954).

(8) E. E. Callaghan and R. S. Ruggeri, "Investigation of the Penetration of an Air Jet Directed Perpendicularly to an Air Stream," NACA TN 1615 (1948).

(9) E. E. Callaghan and D. T. Bowden, "Investigation of Flow Coefficients of Circular, Square, and Elliptical Orifices at High Pressure Ratios," NACA TN 1947 (1949).

(10) R. S. Ruggeri, E. E. Callaghan and D. T. Bowden, "Penetration of Air Jet Issuing from Circular, Square and Elliptical Orifices Directed Perpendicularly to an Air Stream," NACA TN 2019 (1950).

(11) E. E. Callaghan and R. S. Ruggeri, "A General Correlation of Temperature Profiles Downstream of a Heated-Air Jet Directed Perpendicularly to an Air Stream," NACA TN 2466 (1951).

(12) R. S. Ruggeri, "General Correlation of Temperature Profiles Downstream of a Heated Air Jet Directed at Various Angles to Air Stream," NACA TN 2855 (1952).

(13) R. J. Goldstein, E. R. G. Eckert and J. W. Ramsey, "Film Cooling with Injection Through Holes: Adiabatic Wall Temperatures Downstream of a Circular Hole," Journal of Engineering for Power, Trans. ASME Series A, 90, 384-395 (1968).

(14) R. J. Goldstein, E. R. G. Eckert and J. W. Ramsey, "Film Cooling with Injection Through a Circular Hole," NASA CR-54604, May 1968. (Also HTL TR No. 82).

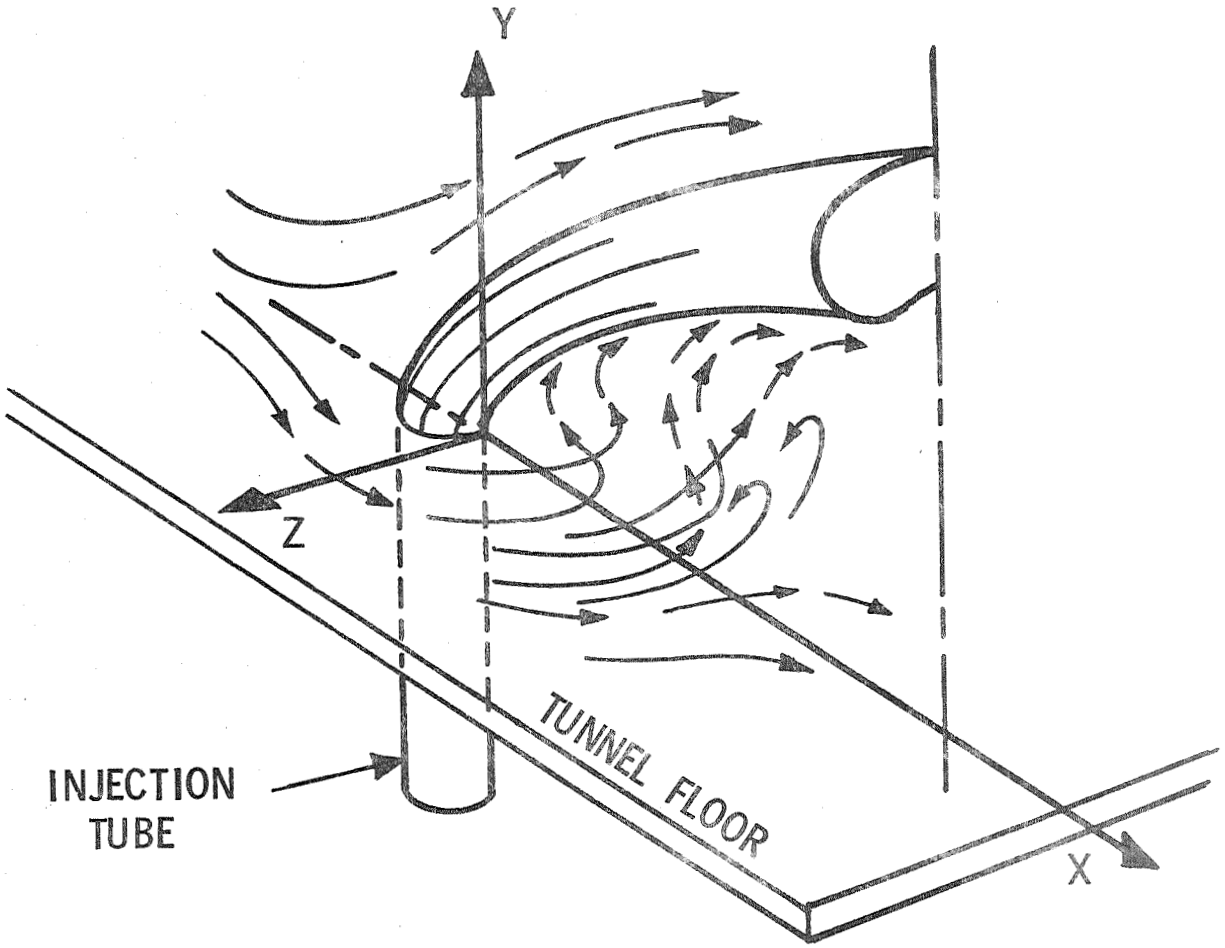

Figure 1 Sketch of half jet based on tuft observations.

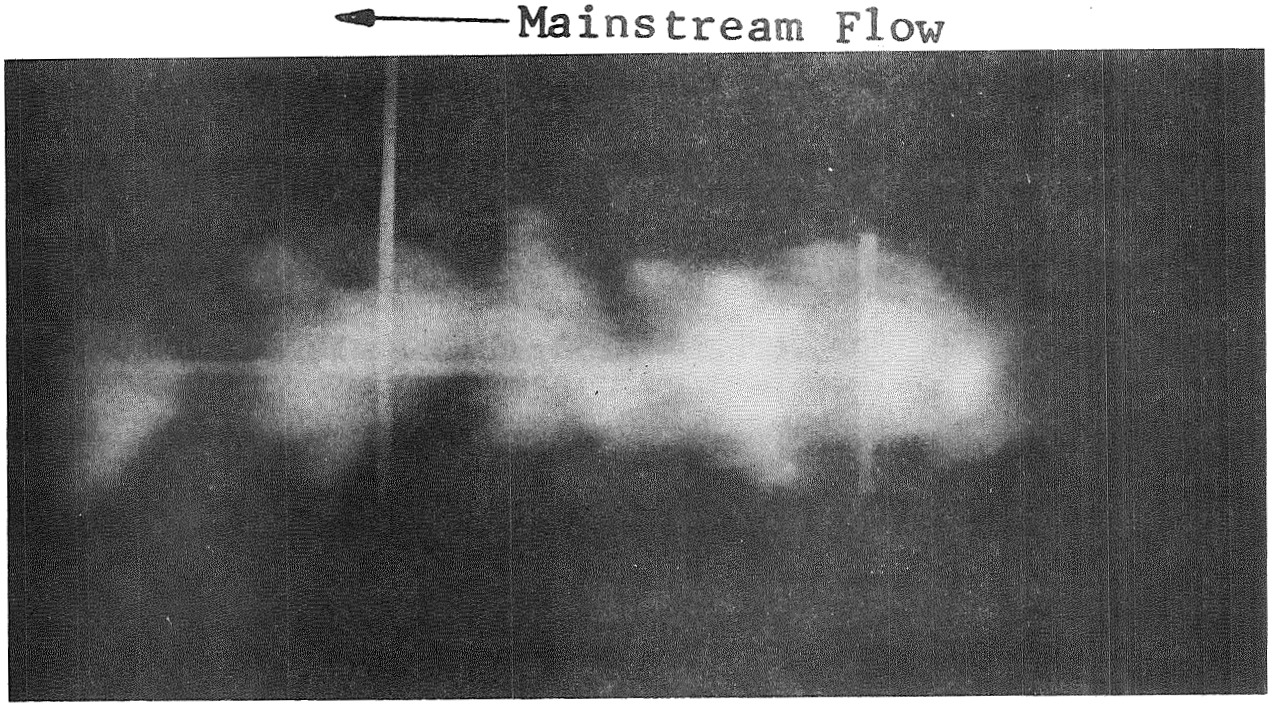

a: exposure time 1/1000 sec

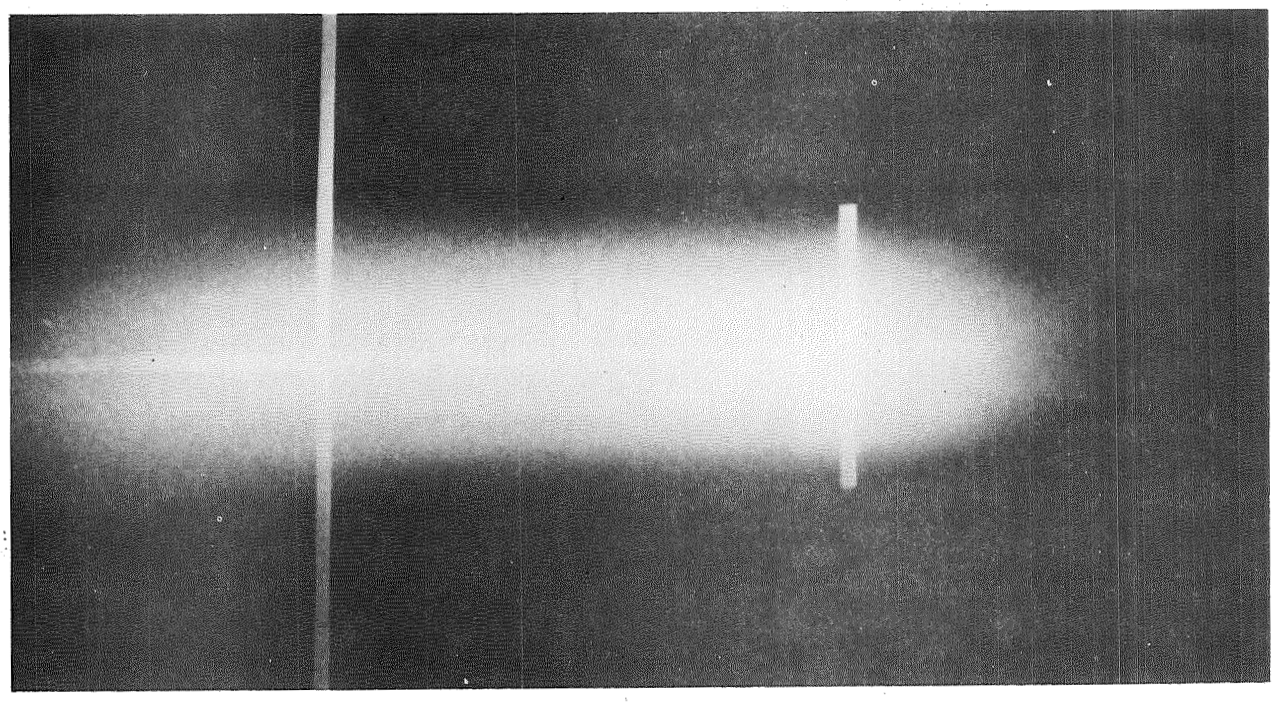

b: exposure time 1/8 sec

BLOWING RATE, M = 1

Figure 2 Flow visualization of jet entering free stream.

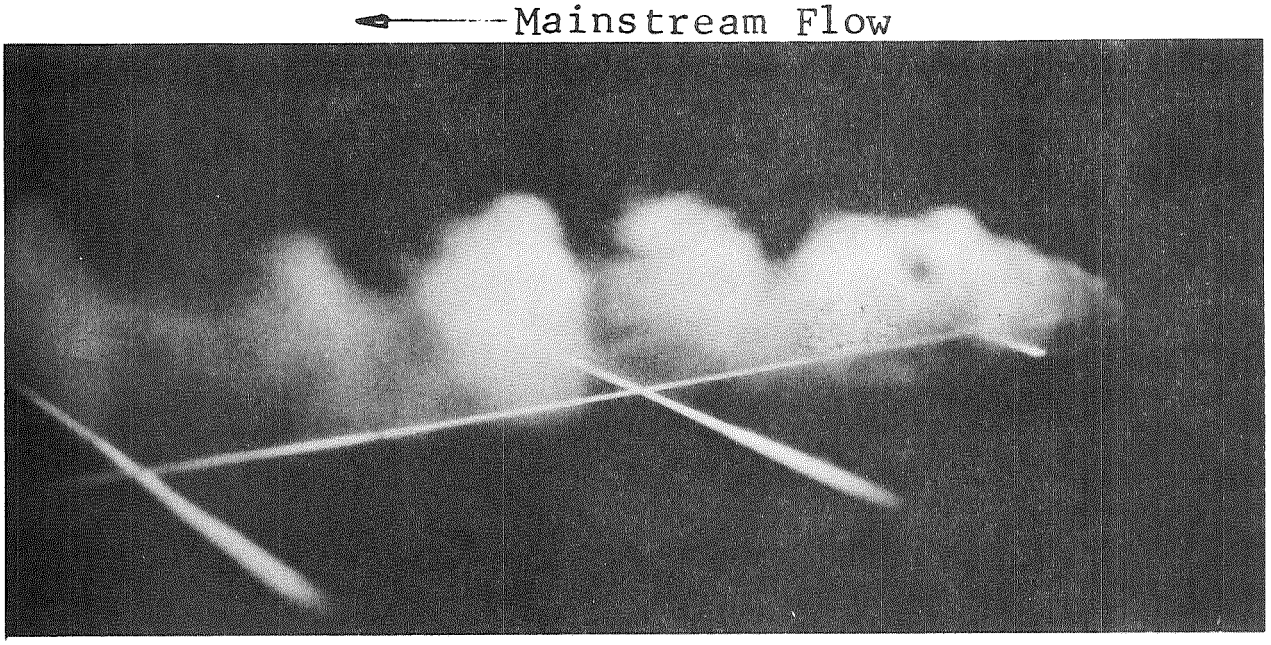

c: exposure time 1/1000 sec

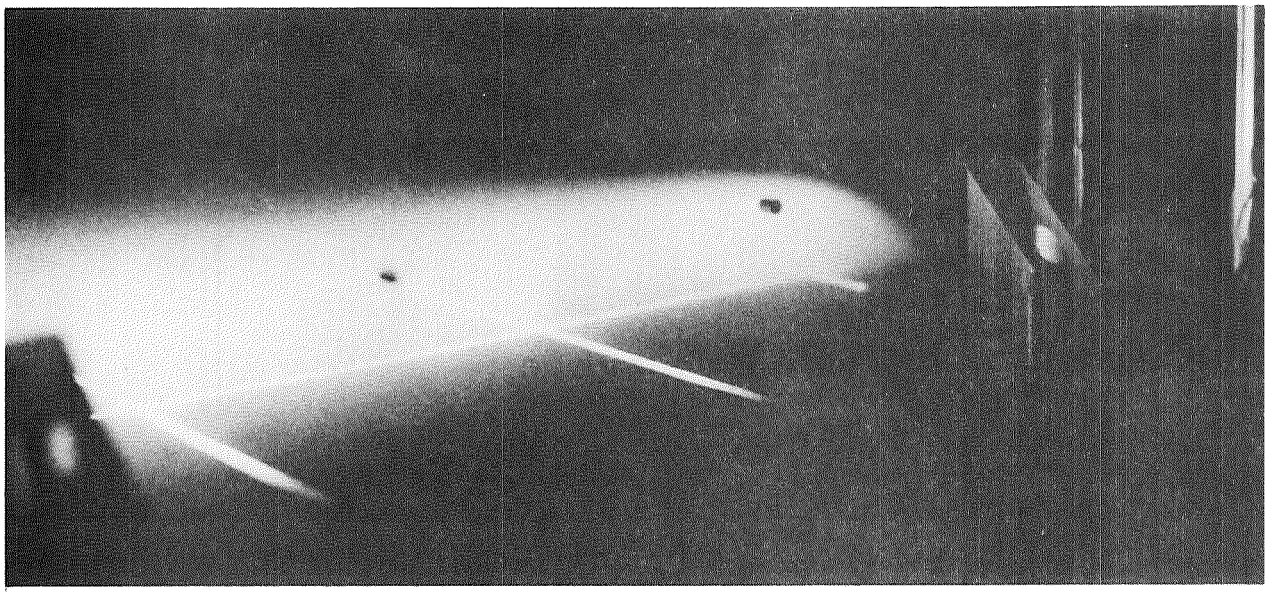

d: exposure time 1/8 sec

BLOWING RATE, M = 0.9

Figure 2 concluded

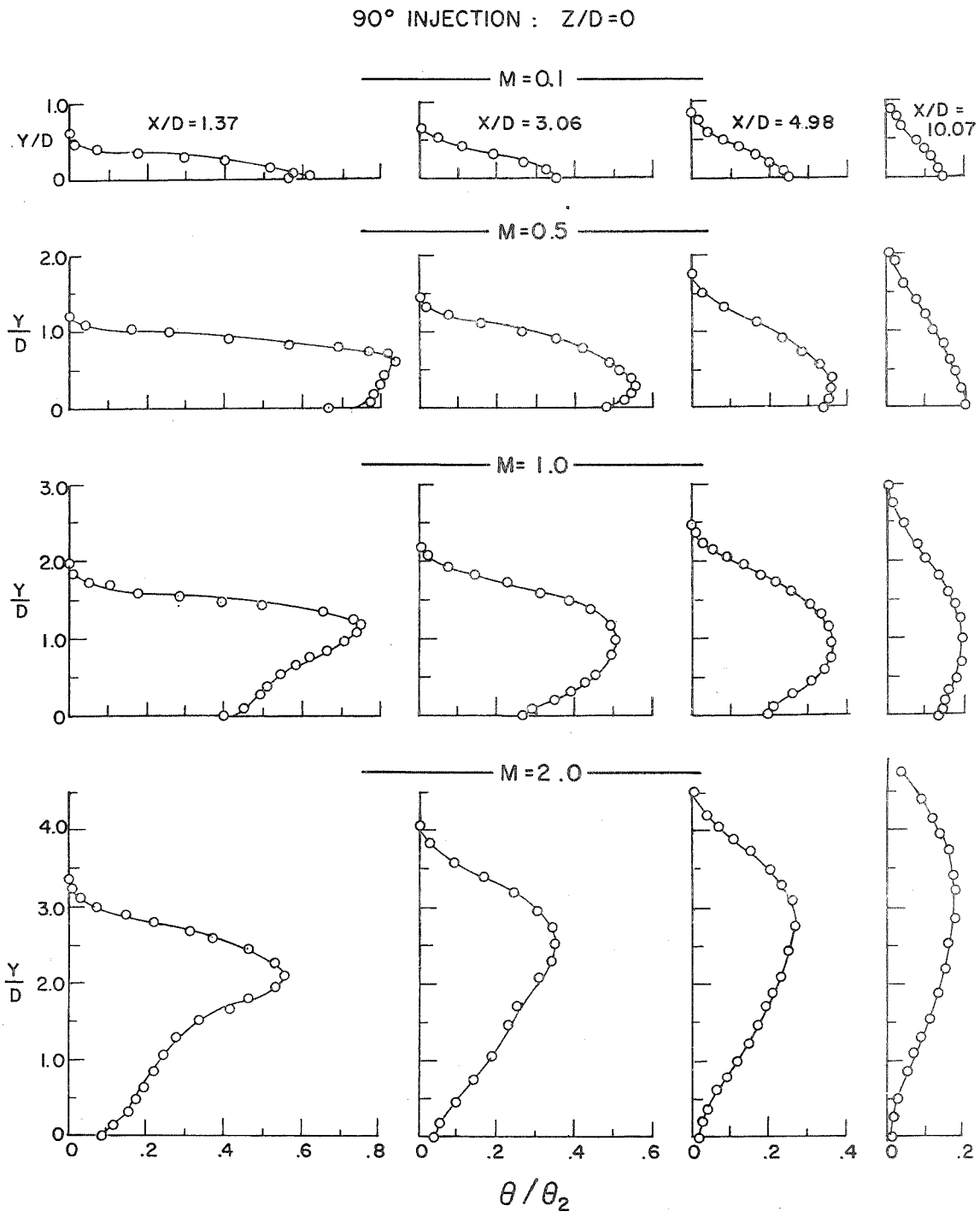

Figure 3 Temperature profiles for 90° injection angle, Z/D=0.

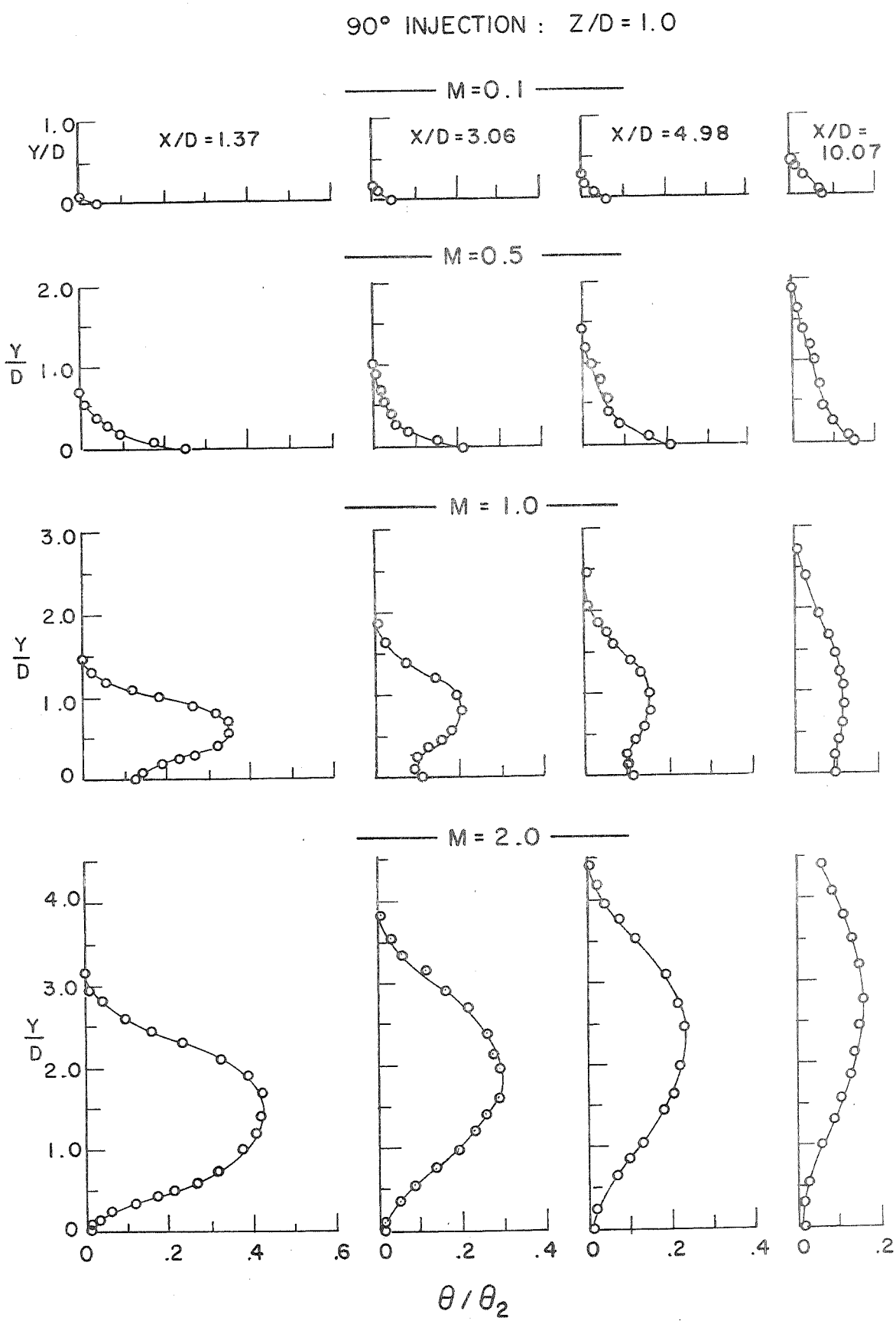

Figure 4 Temperature profiles for 90° injection angle, Z/D=1.

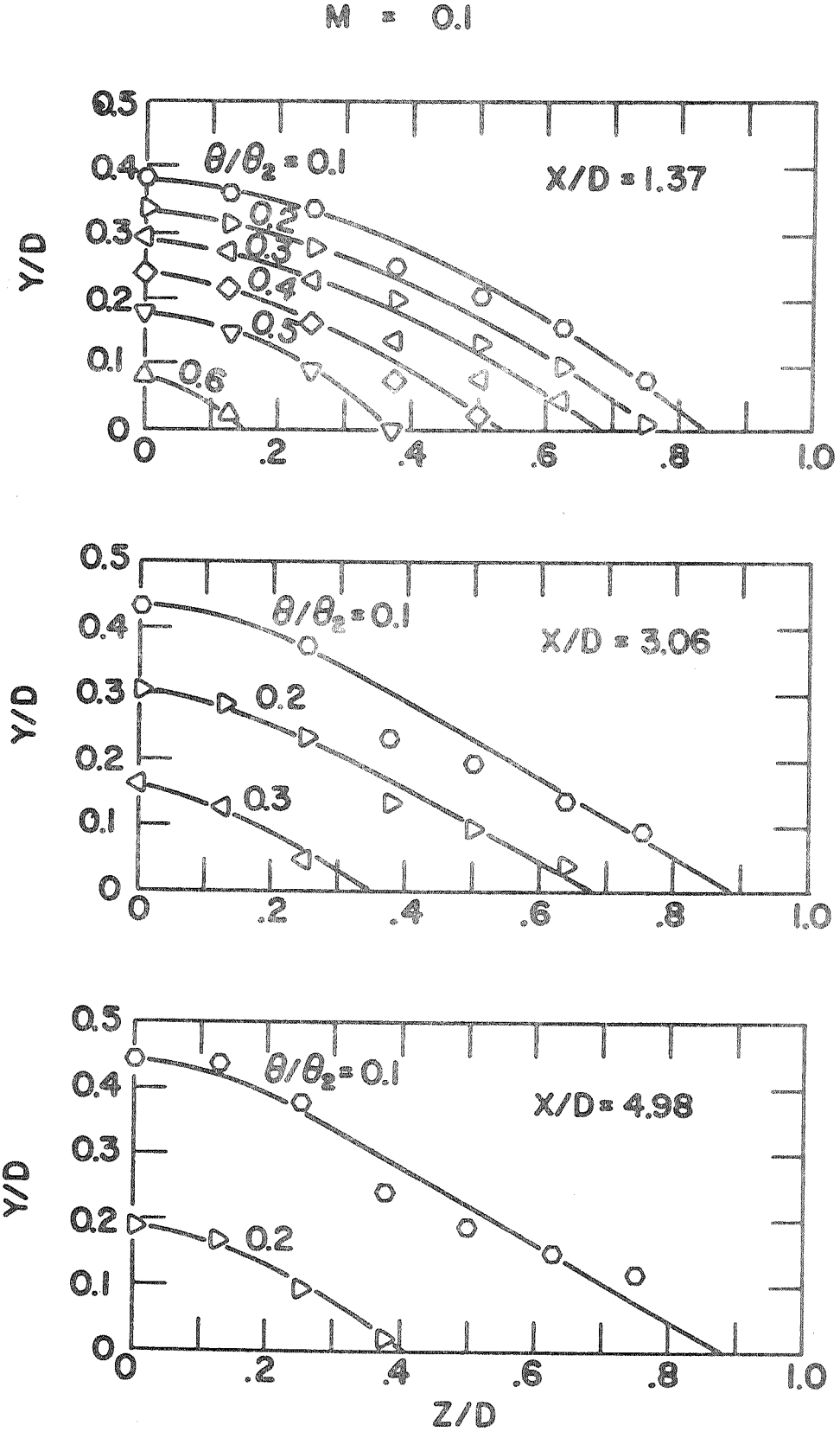

Figure 5 Constant temperature contours for 90° injection angle, M=0.1.

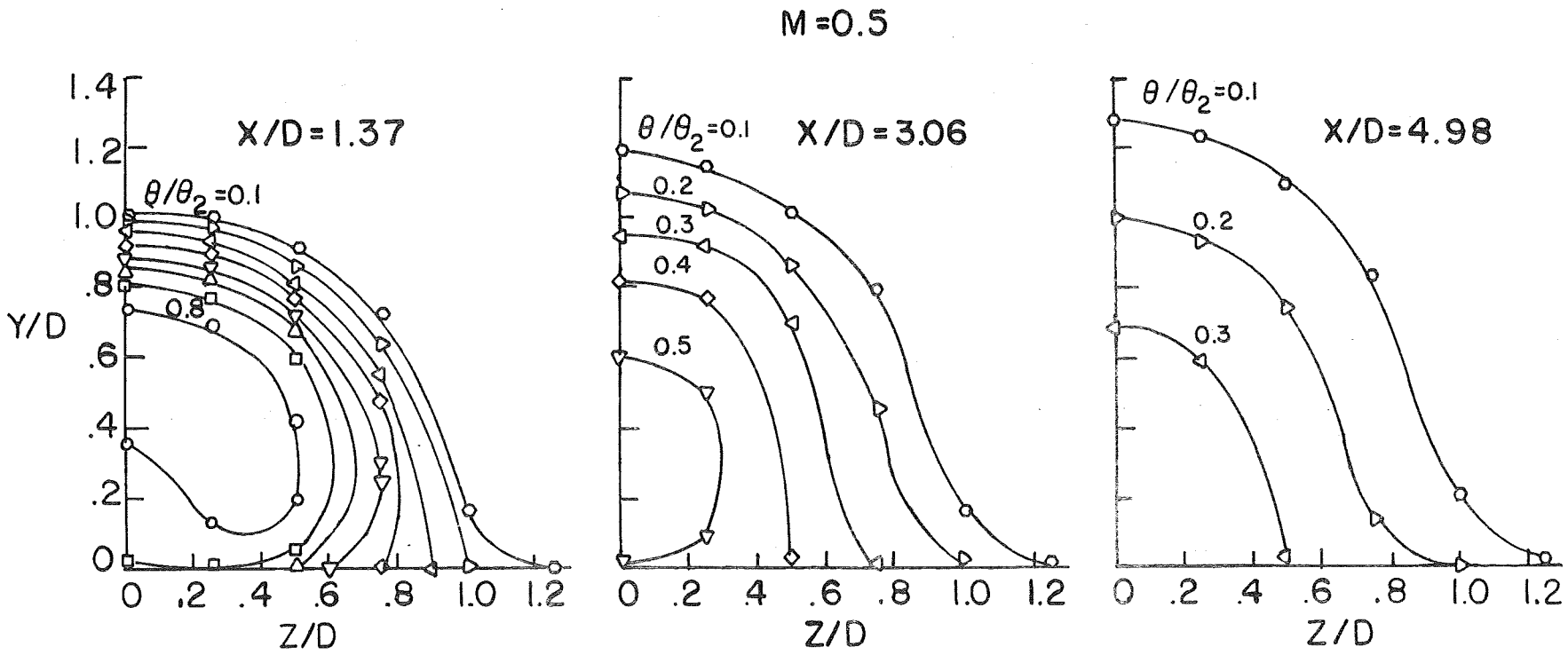

Figure 6 Constant temperature contours for 90° injection angle, M=0.5.

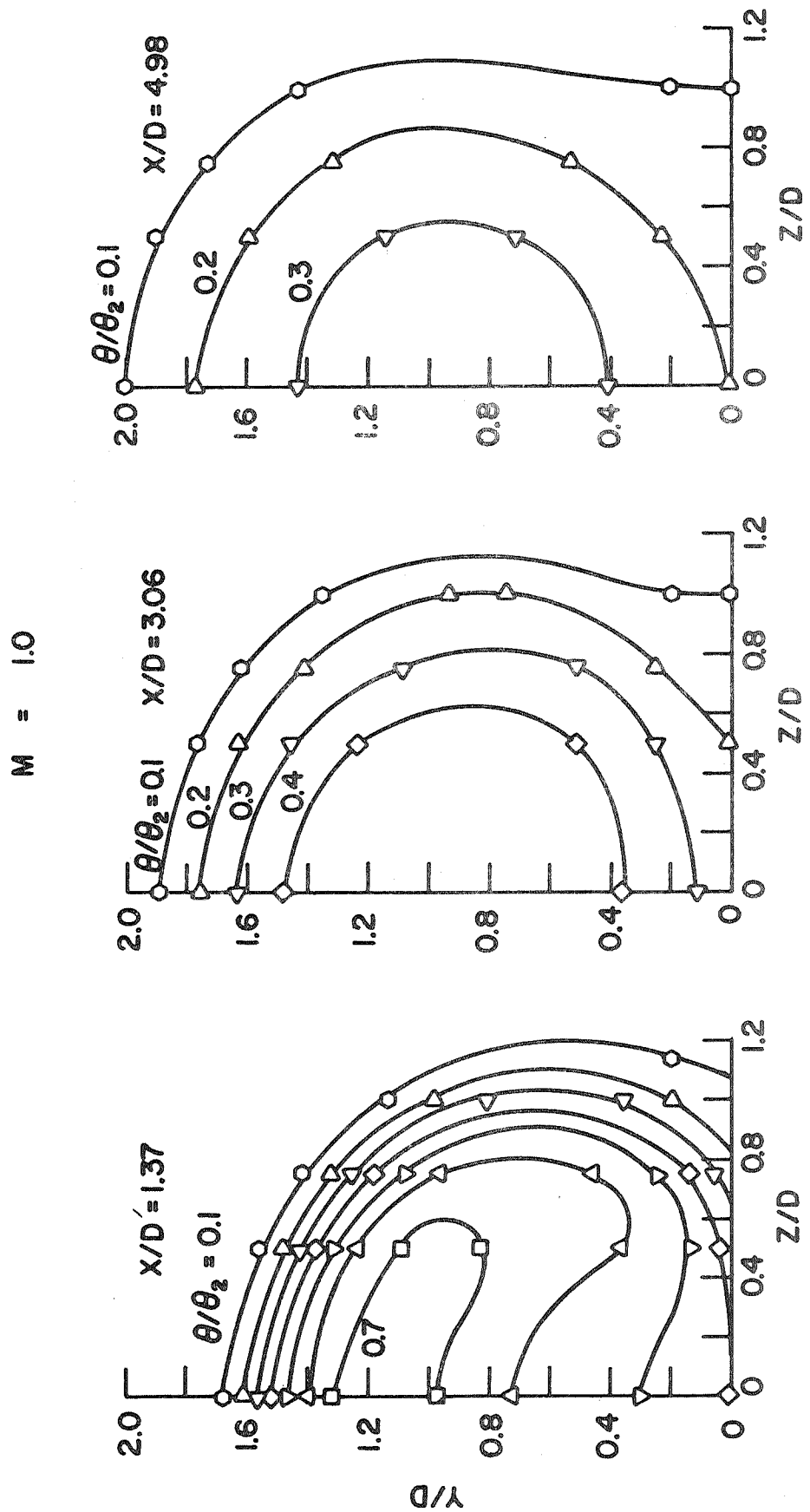

Figure 7 Constant temperature contours for 90^{o} injection angle, M=1.0.

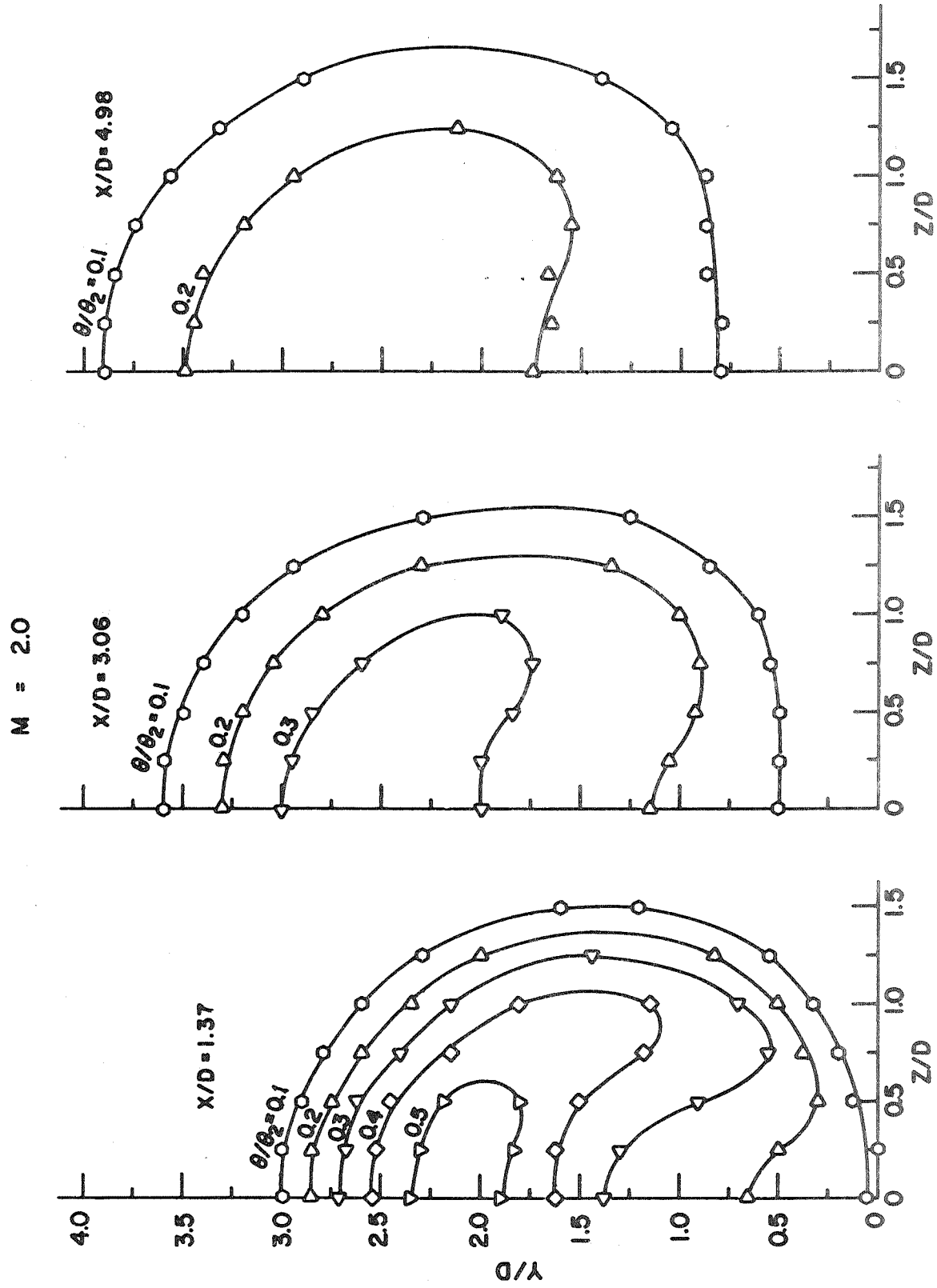

Figure 8 Constant temperature contours for 90° injection angle, M=2.0.

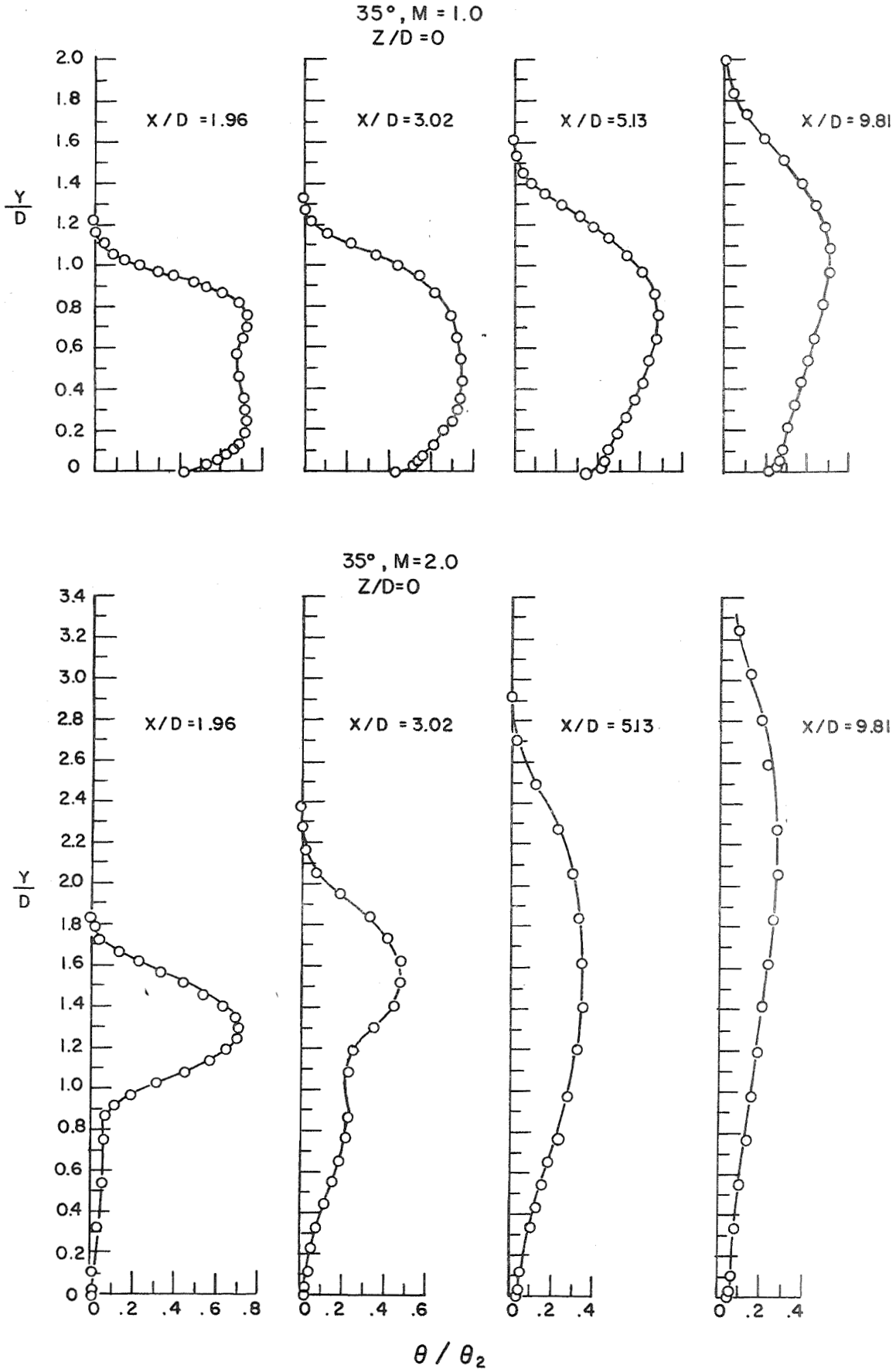

Figure 9 Temperature profiles for 35^{o} injection angle, Z/D=0.

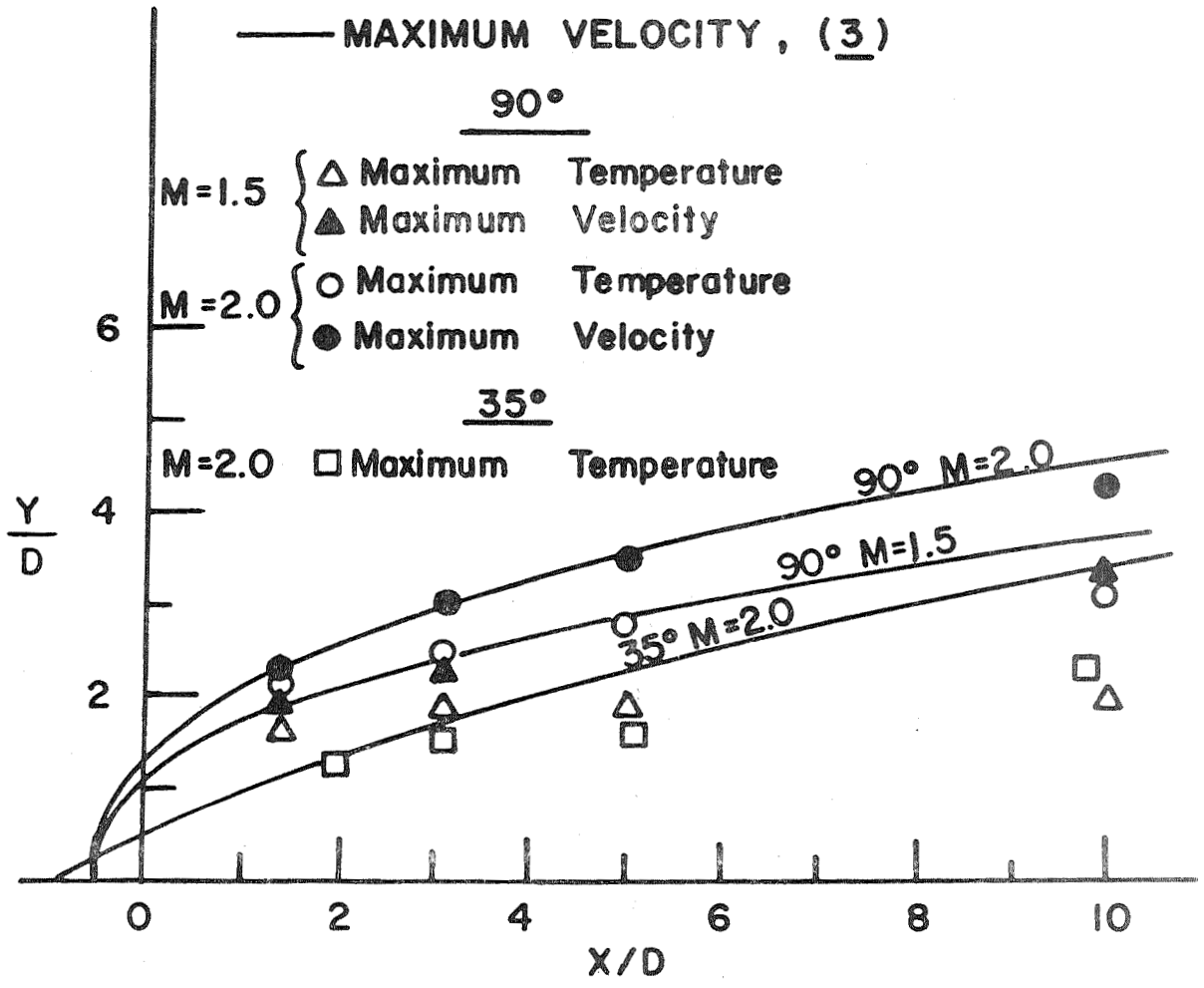

Figure 10 Positions of maximum temperature and velocity as a function of axial position for 90° and 35° injection angles, Z/D=0, M=1.5 and 2.0.

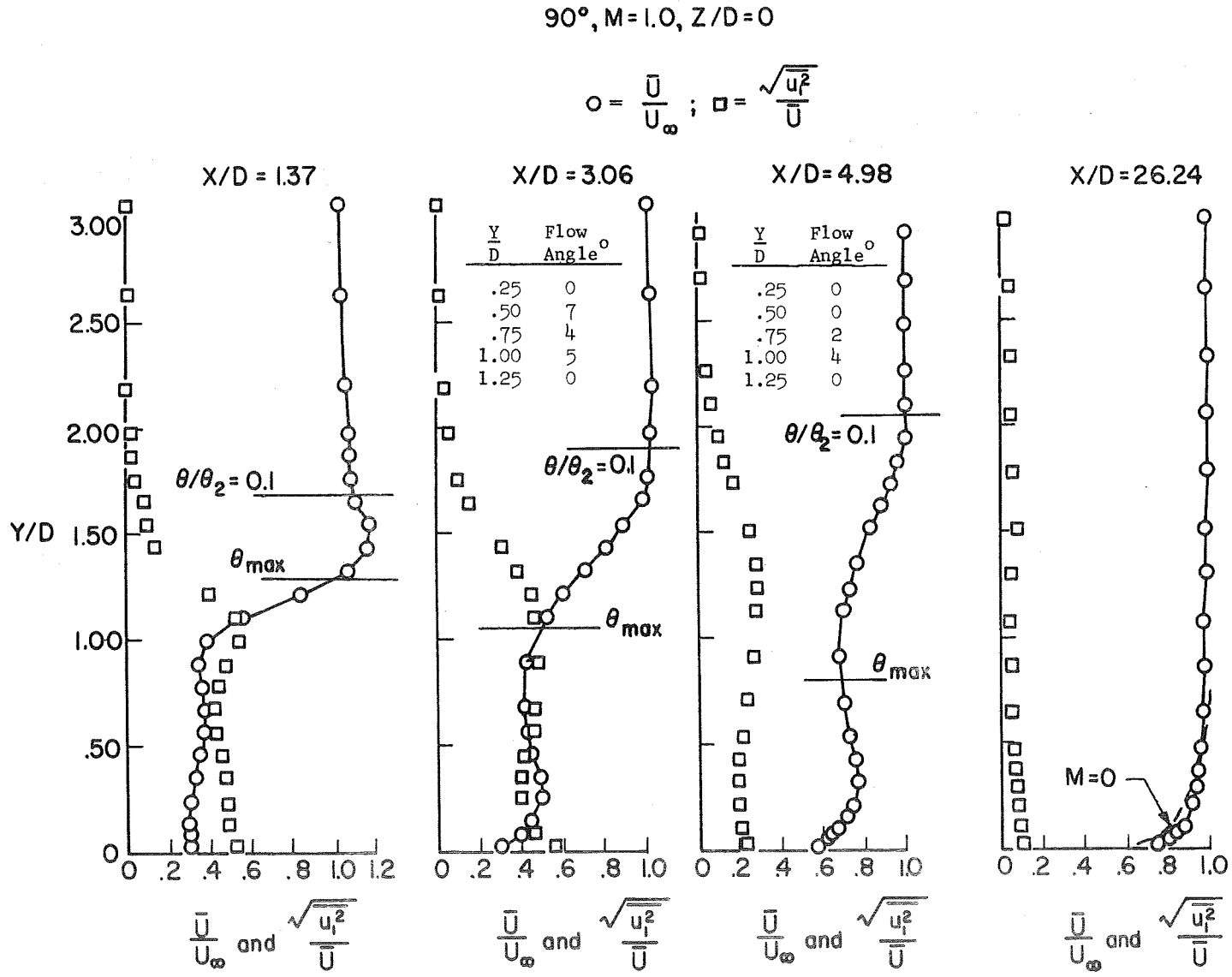

Figure 11 Velocity and turbulence intensity profiles for 90° injection angle, Z/D=0, M=1.0.

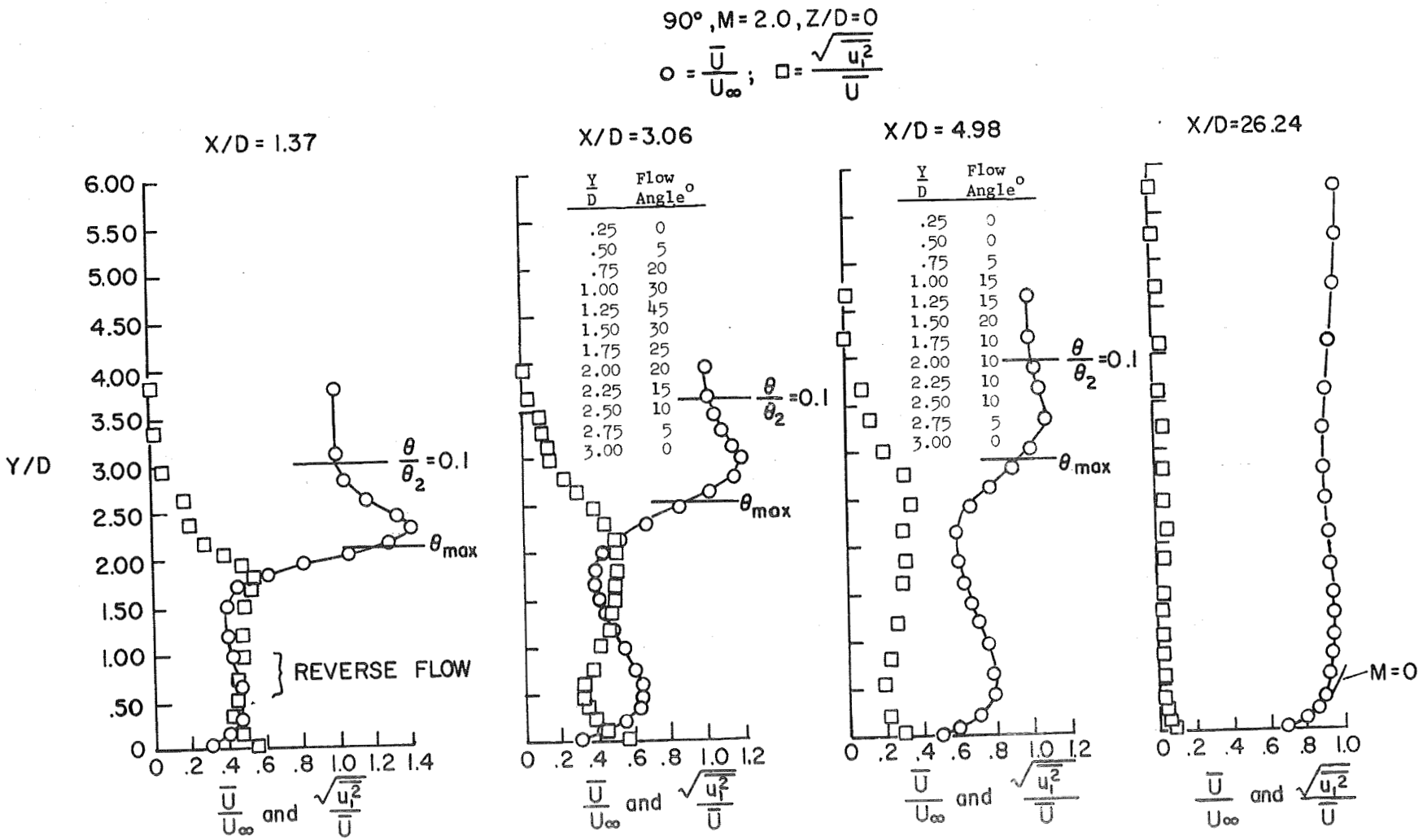

Figure 12 Velocity and turbulence intensity profiles for 90° injection angle, Z/D=0, M=2.0.

APPENDIX

Contained herein are additional curves showing details of temperature and velocity profiles obtained under various conditions in terms of blowing rate, angle of injection, and position along the flow. Parts of some of these figures have been used within the body of this report, but they are presented again for the sake of completeness in this appendix. A table representing the parameters of the different figures is as presented below.

Figure	Angle of Injection	Blowing Rate, M	Profile Shown
A1a&b	90^{o}	0.1	Temperature
A2a,b&c	90^{o}	0.2	Temperature
A3a,b&c	90^{o}	0.5	Temperature
A4a,b&c	90^{o}	0.77	Temperature
A5a&b	90^{o}	1.0	Temperature
A6a,b,c&d	90^{o}	1.5	Temperature
A7a,b,c&d	90^{o}	2.0	Temperature
A8a&b	35^{o}	1.0	Temperature
A9a,b&c	35^{o}	2.0	Temperature
A10a,b&c	90^{o}	1.0	Velocity
A11	90^{o}	1.5	Velocity
A12a&b	90^{o}	2.0	Velocity

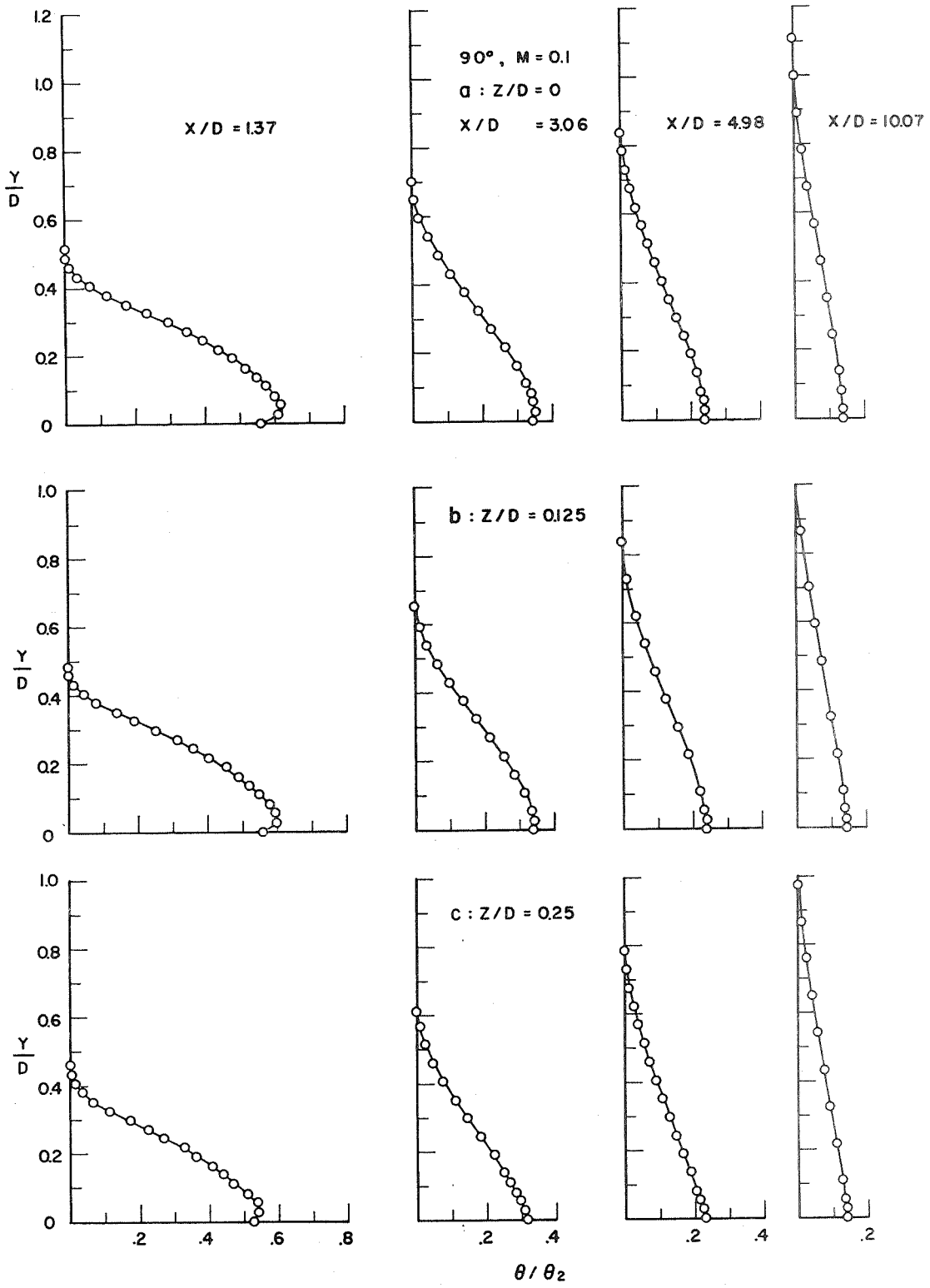

Figure A1a Temperature profiles for 90° injection angle, M=0.1.

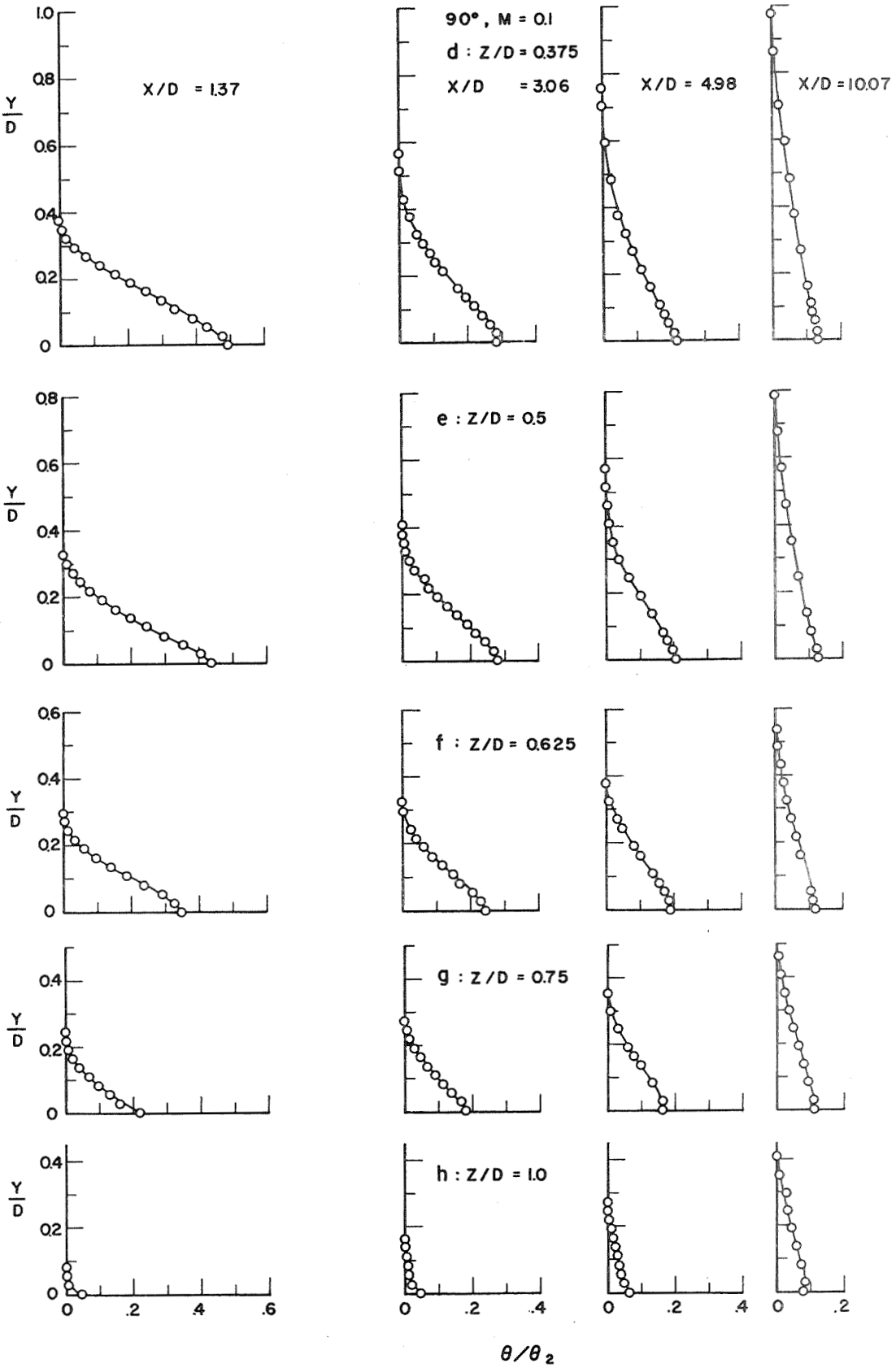
90°, M = 0.1
d : Z/D = 0.375
X/D = 3.06
X/D = 1.37
X/D = 4.98
X/D = 10.07
e : Z/D = 0.5
f : Z/D = 0.625
g : Z/D = 0.75
h : Z/D = 1.0
Y/D
θ/θ2

Figure A1b

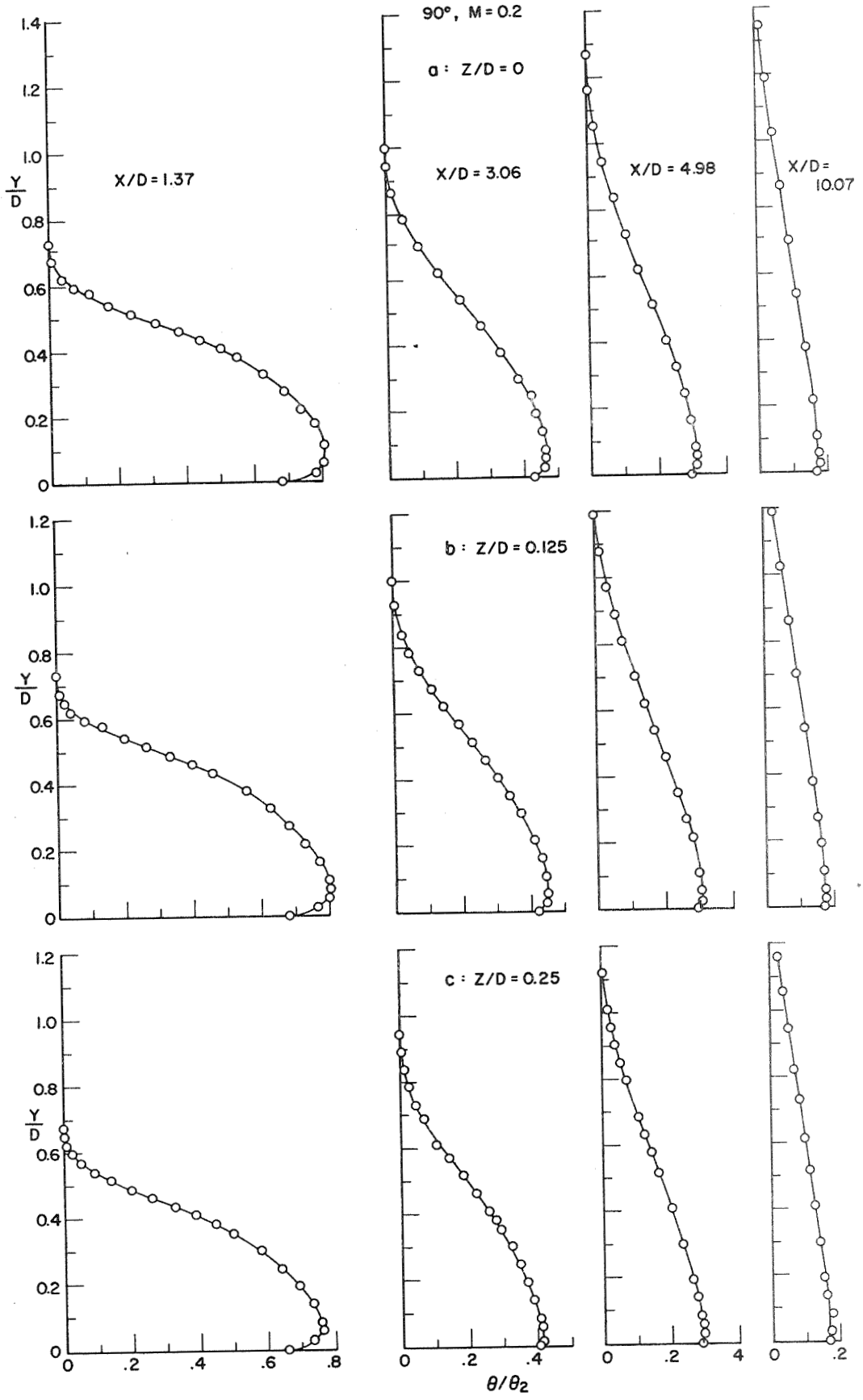

Figure A2a Temperature profiles for 90° injection angle, M=0.2.

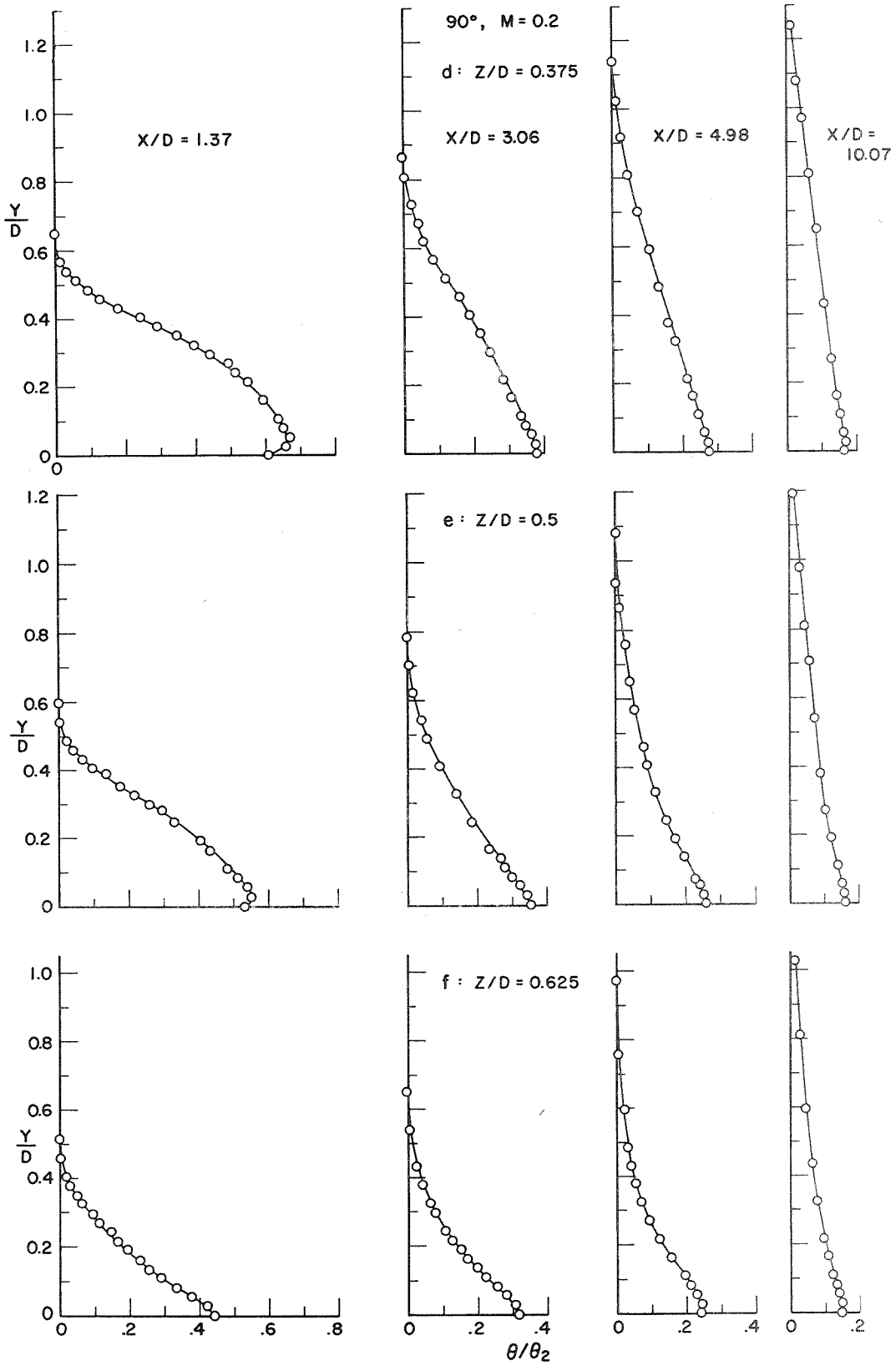
90°, M = 0.2
d : Z/D = 0.375
e : Z/D = 0.5
f : Z/D = 0.625
X/D = 1.37
X/D = 3.06
X/D = 4.98
X/D = 10.07
Y/D
θ/θ2

Figure A2b

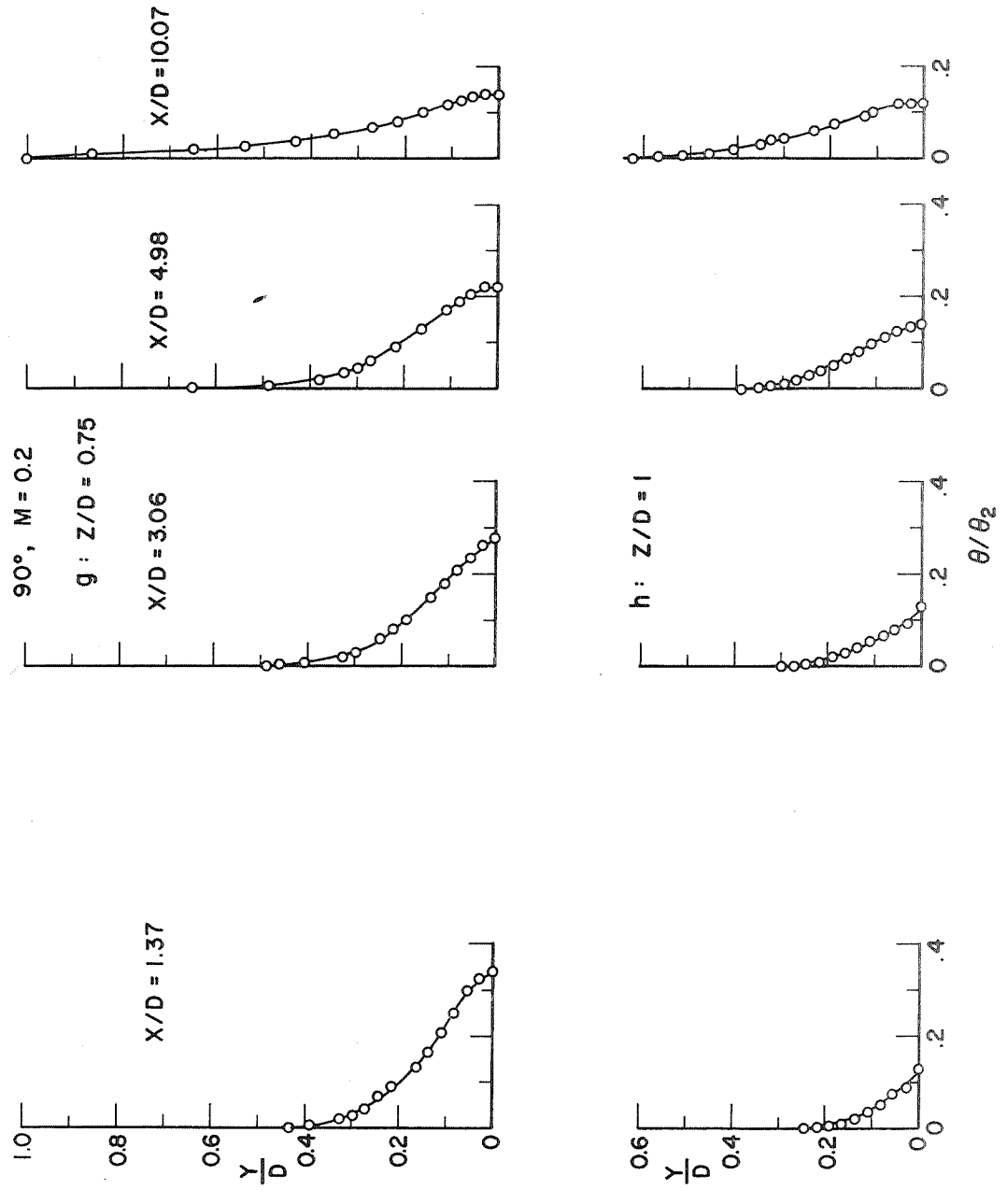
90°, M = 0.2
g : Z/D = 0.75
h : Z/D = 1
X/D = 1.37
X/D = 3.06
X/D = 4.98
X/D = 10.07
Y/D
θ/θ2
0
0.2
0.4
0.6
0.8
1.0

Figure A2c

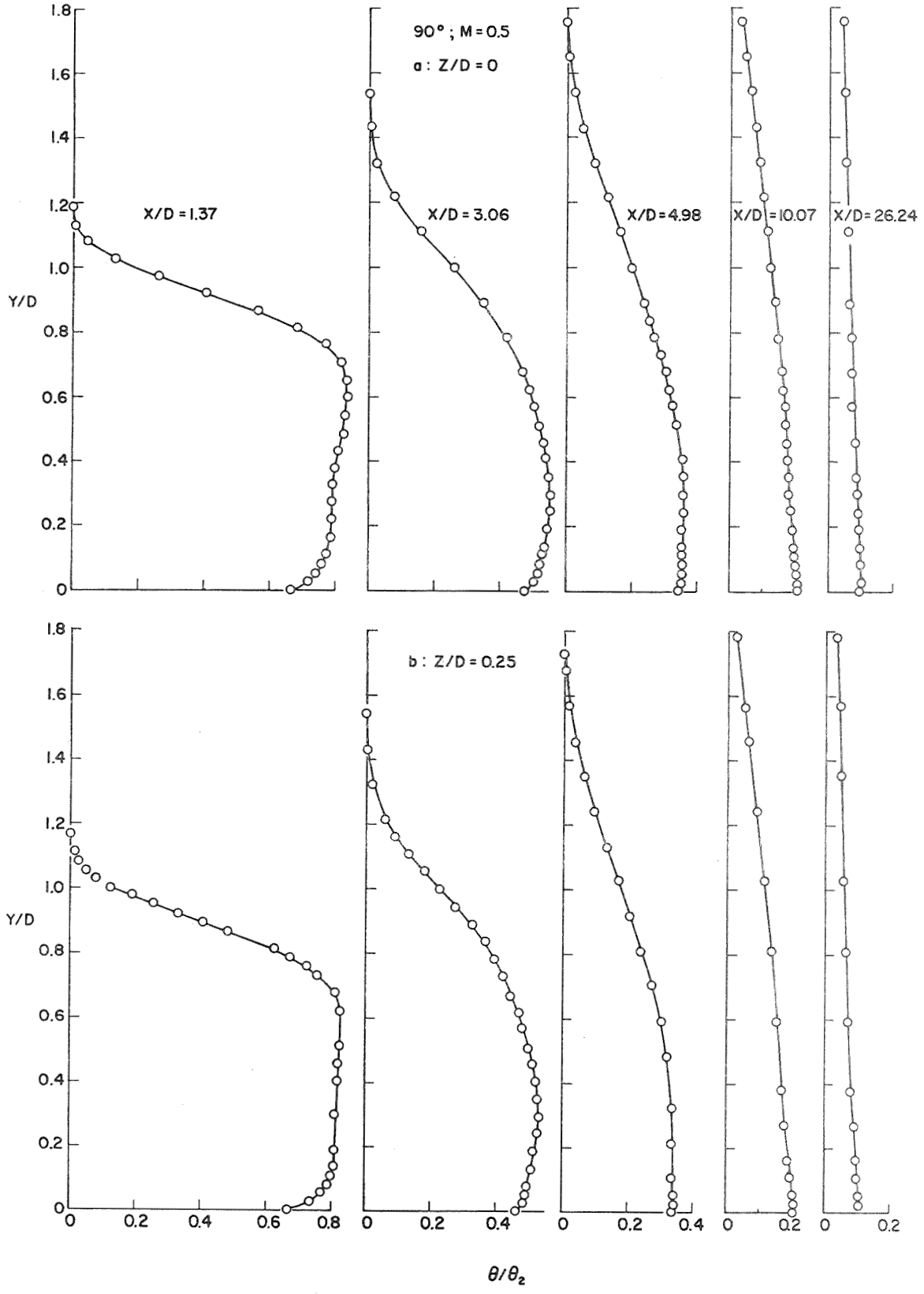

Figure A3a Temperature profiles for 90^{o} injection angle, M=0.5.

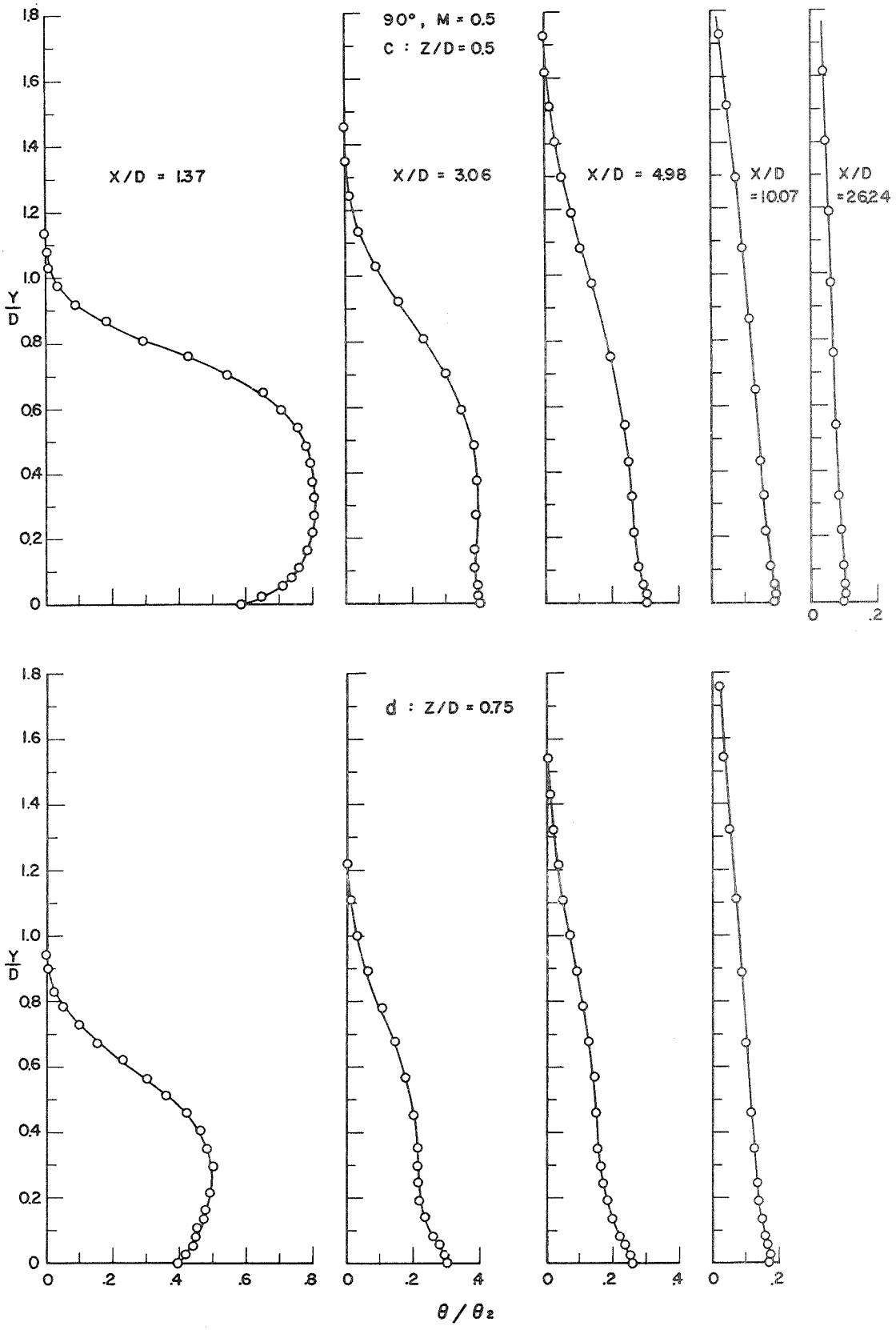

Figure A3b

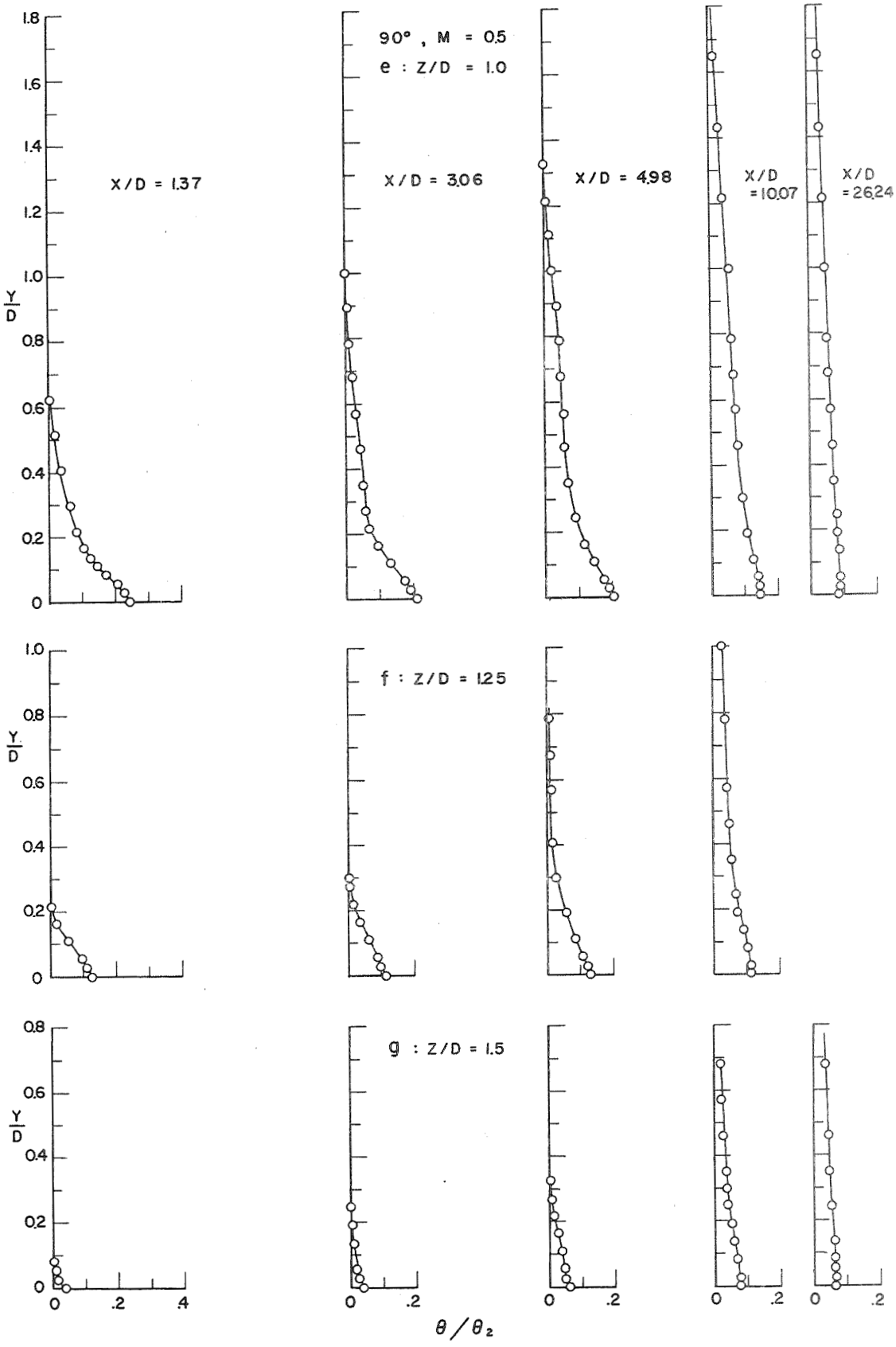
90° , M = 0.5
e : Z/D = 1.0
X/D = 1.37
X/D = 3.06
X/D = 4.98
X/D = 10.07
X/D = 26.24
f : Z/D = 1.25
g : Z/D = 1.5
Y/D
θ/θ₂

Figure A3c

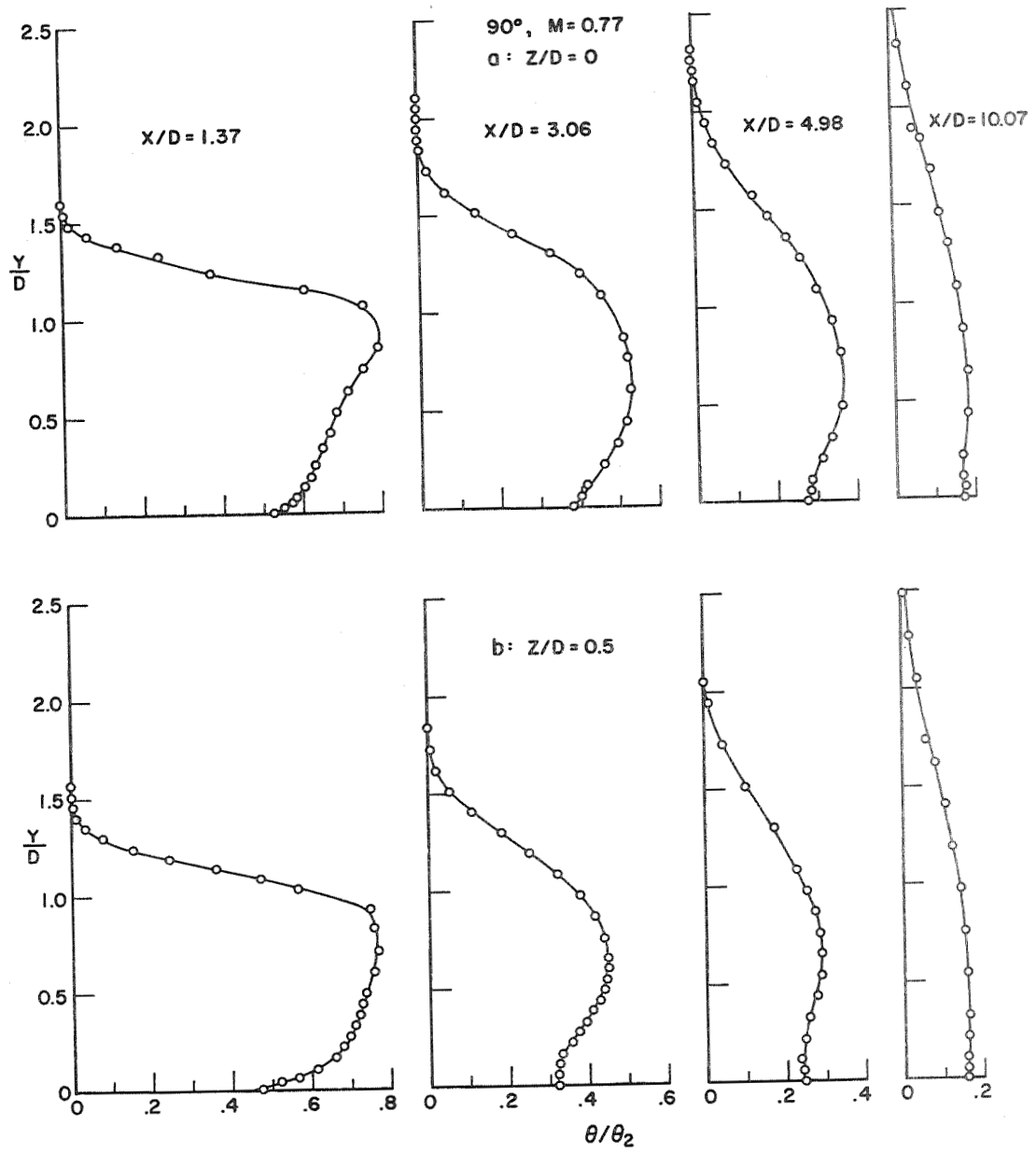

Figure A4a Temperature profiles for 90° injection angle, M=0.77.

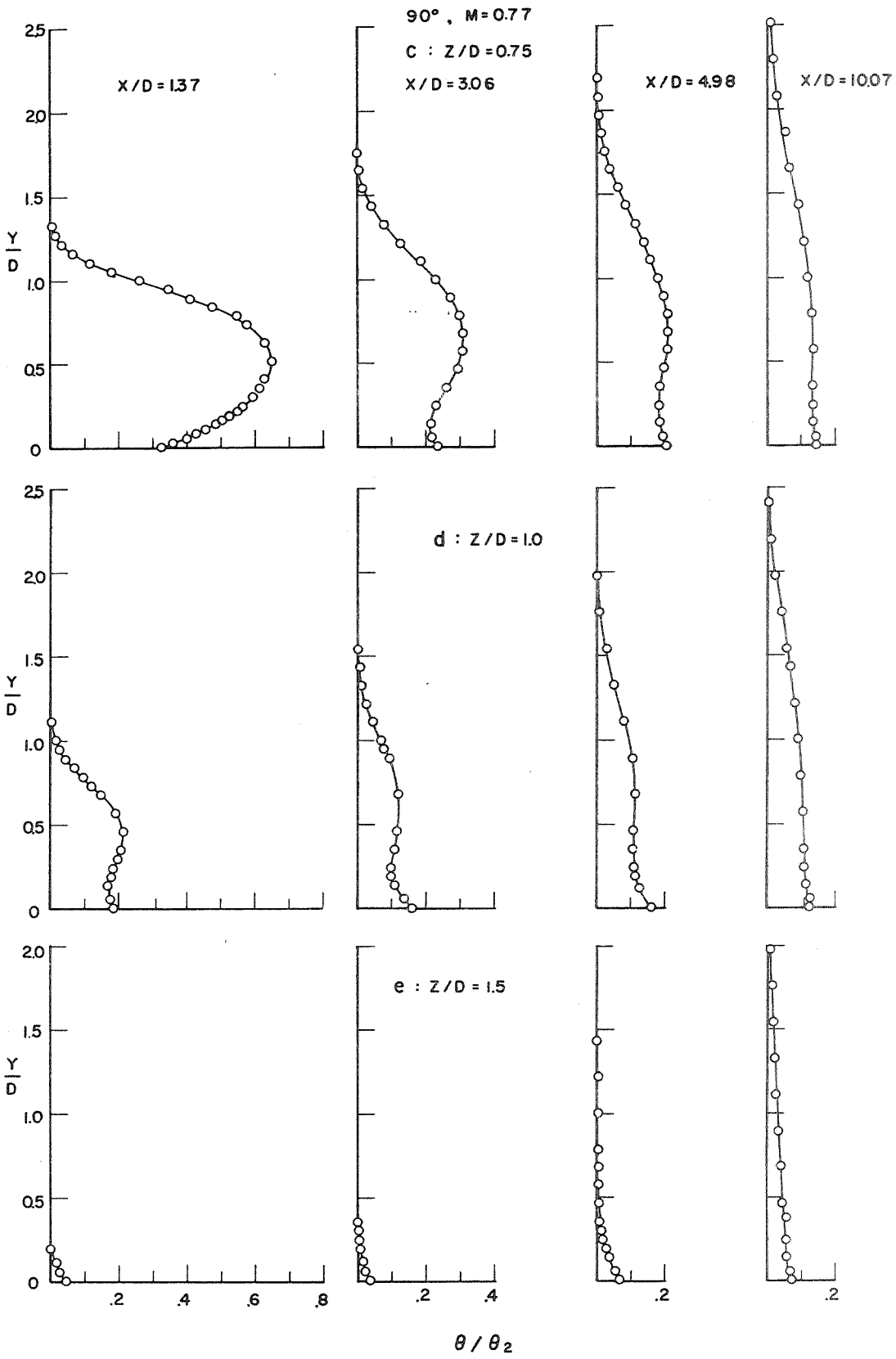

Figure A4b

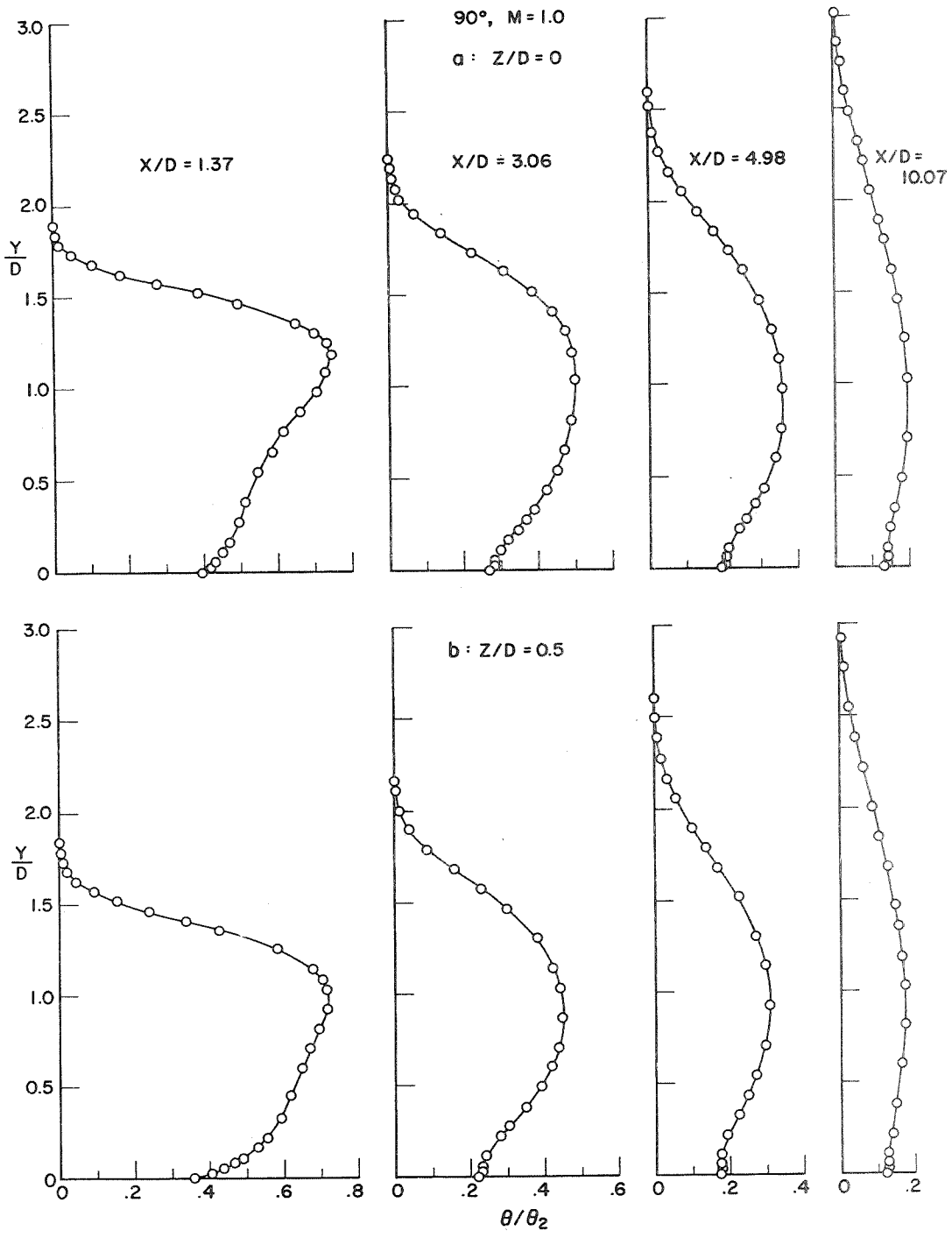

Figure A5a Temperature profiles for 90° injection angle, M=1.0.

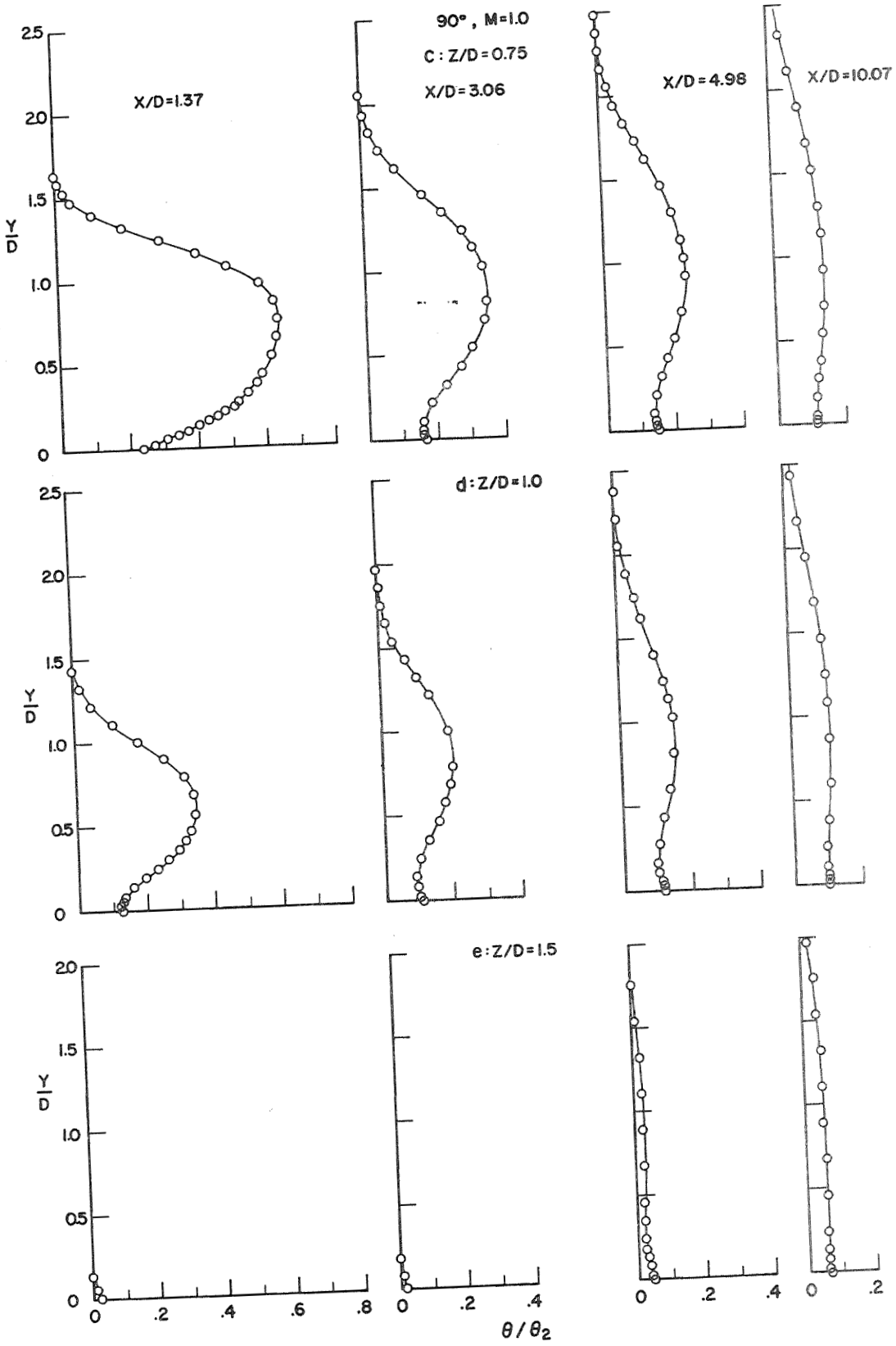

Figure A5b

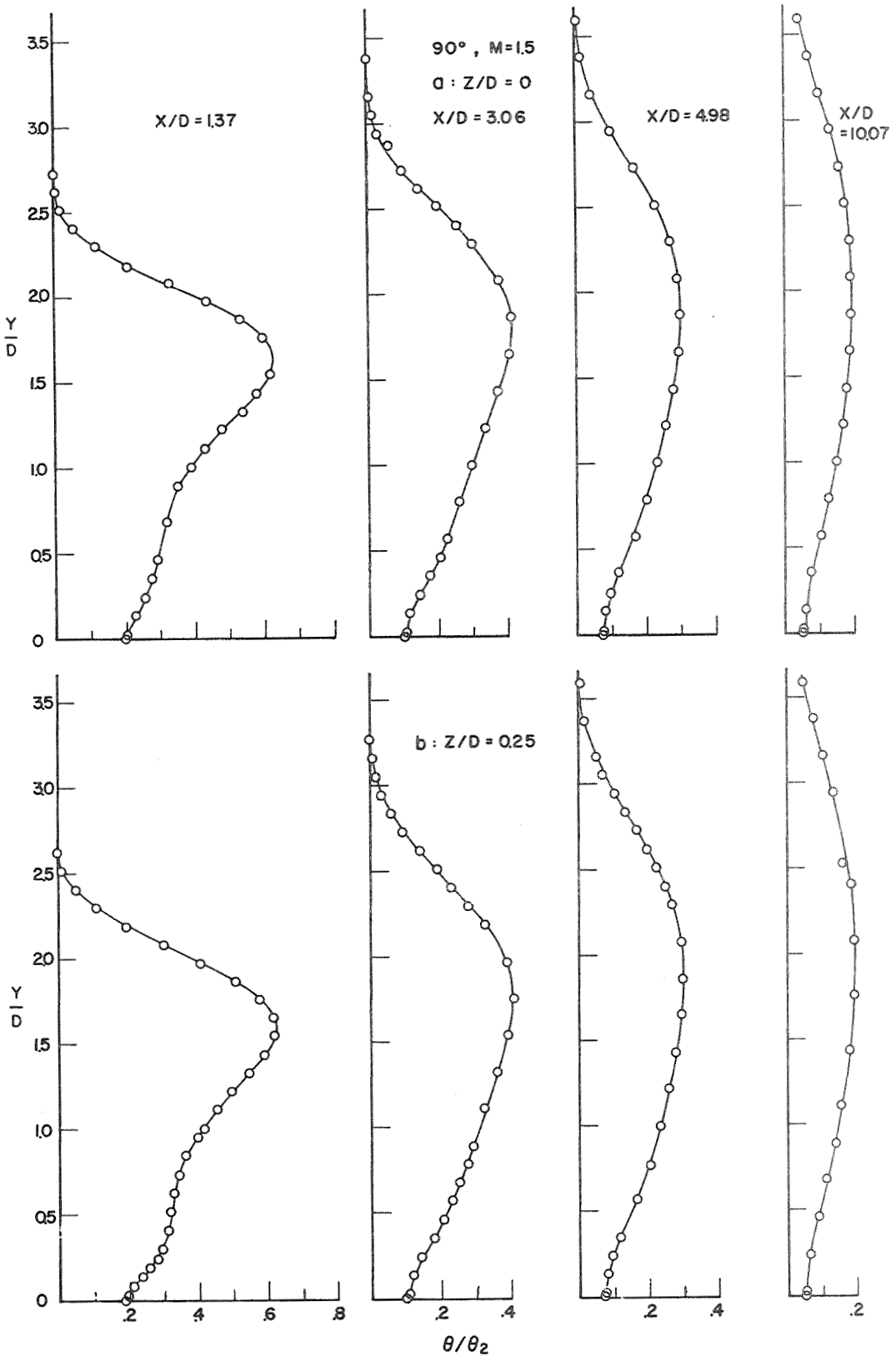

Figure A6a Temperature profiles for 90° injection angle, M=1.5.

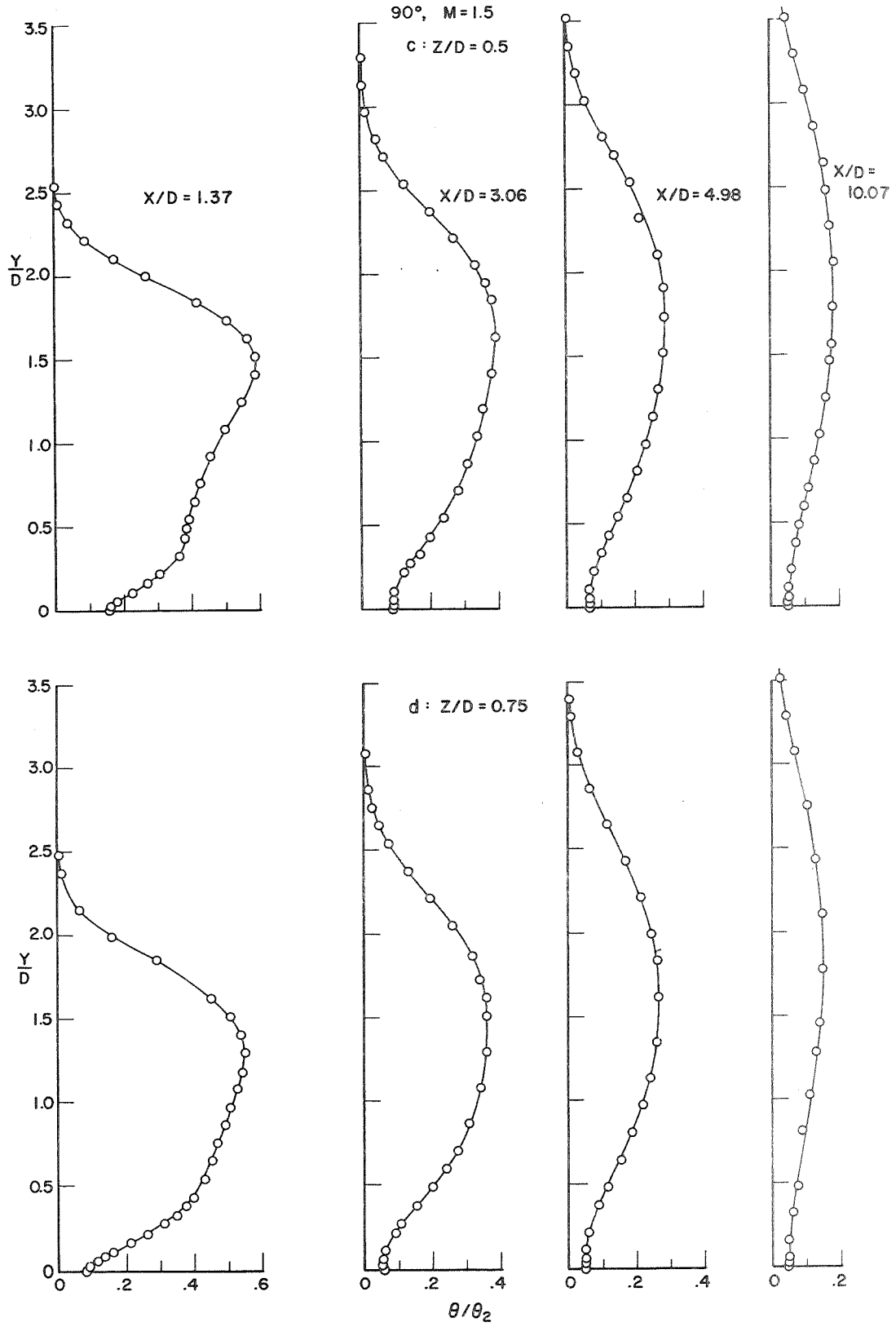

Figure A6b

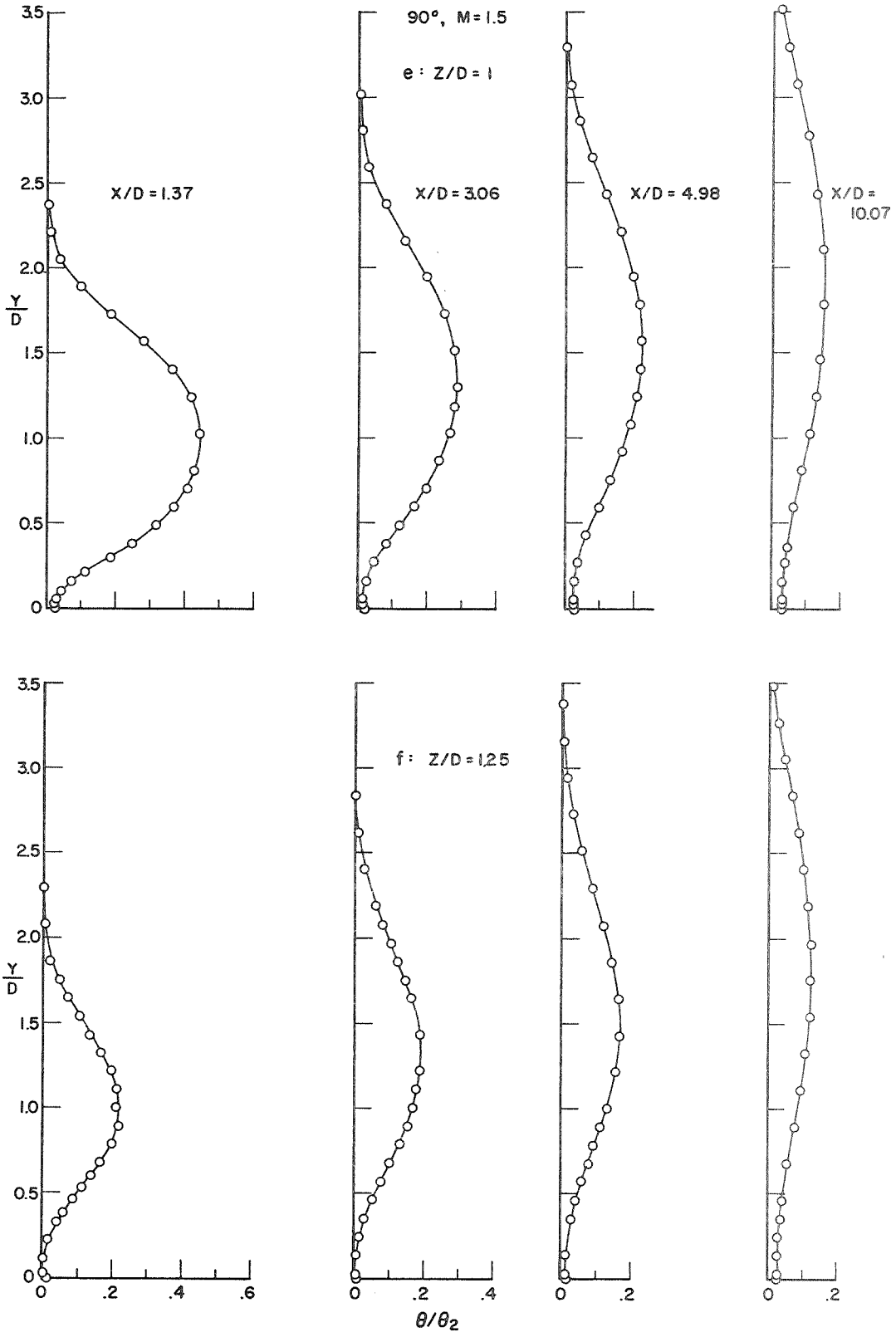
90°, M = 1.5
e : Z/D = 1
f : Z/D = 1.25
X/D = 1.37
X/D = 3.06
X/D = 4.98
X/D = 10.07
Y/D
θ/θ2
0
0.5
1.0
1.5
2.0
2.5
3.0
3.5
.2
.4
.6

Figure A6c

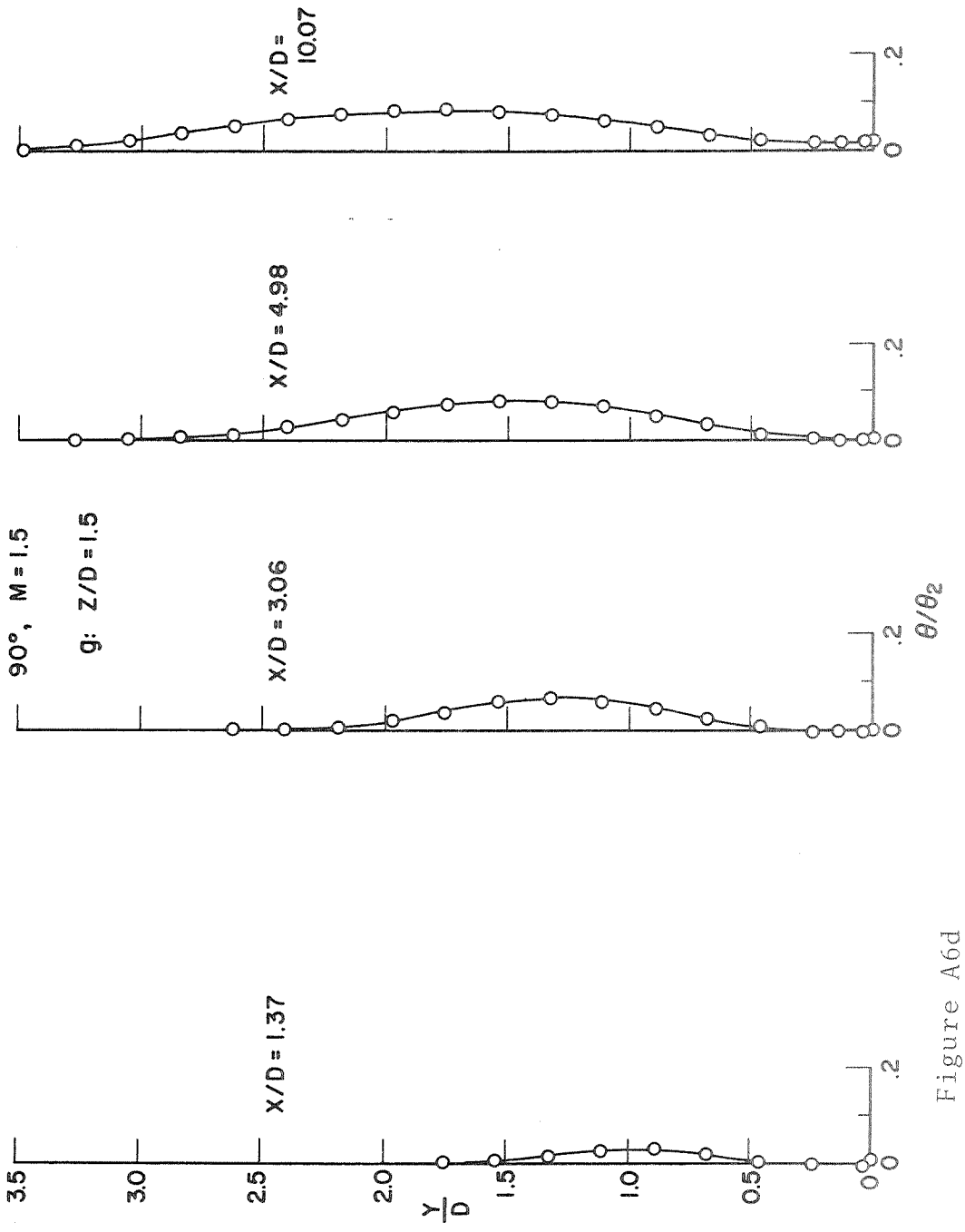
90°, M = 1.5
g: Z/D = 1.5
X/D = 1.37
X/D = 3.06
X/D = 4.98
X/D = 10.07
Y/D
θ/θ2
0
0.5
1.0
1.5
2.0
2.5
3.0
3.5
.2

Figure A6d

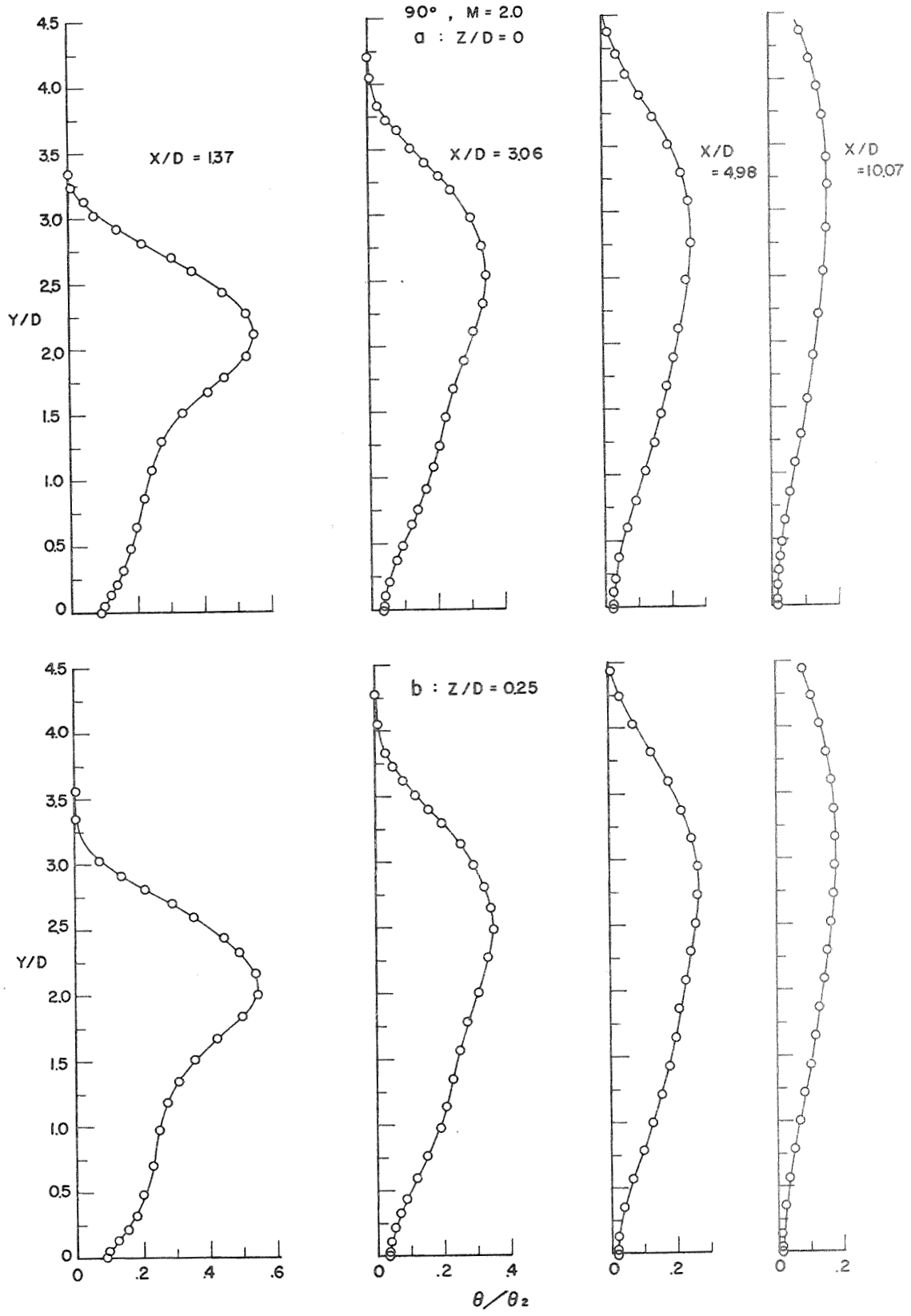

Figure A7a Temperature profiles for 90° injection angle, M=2.0.

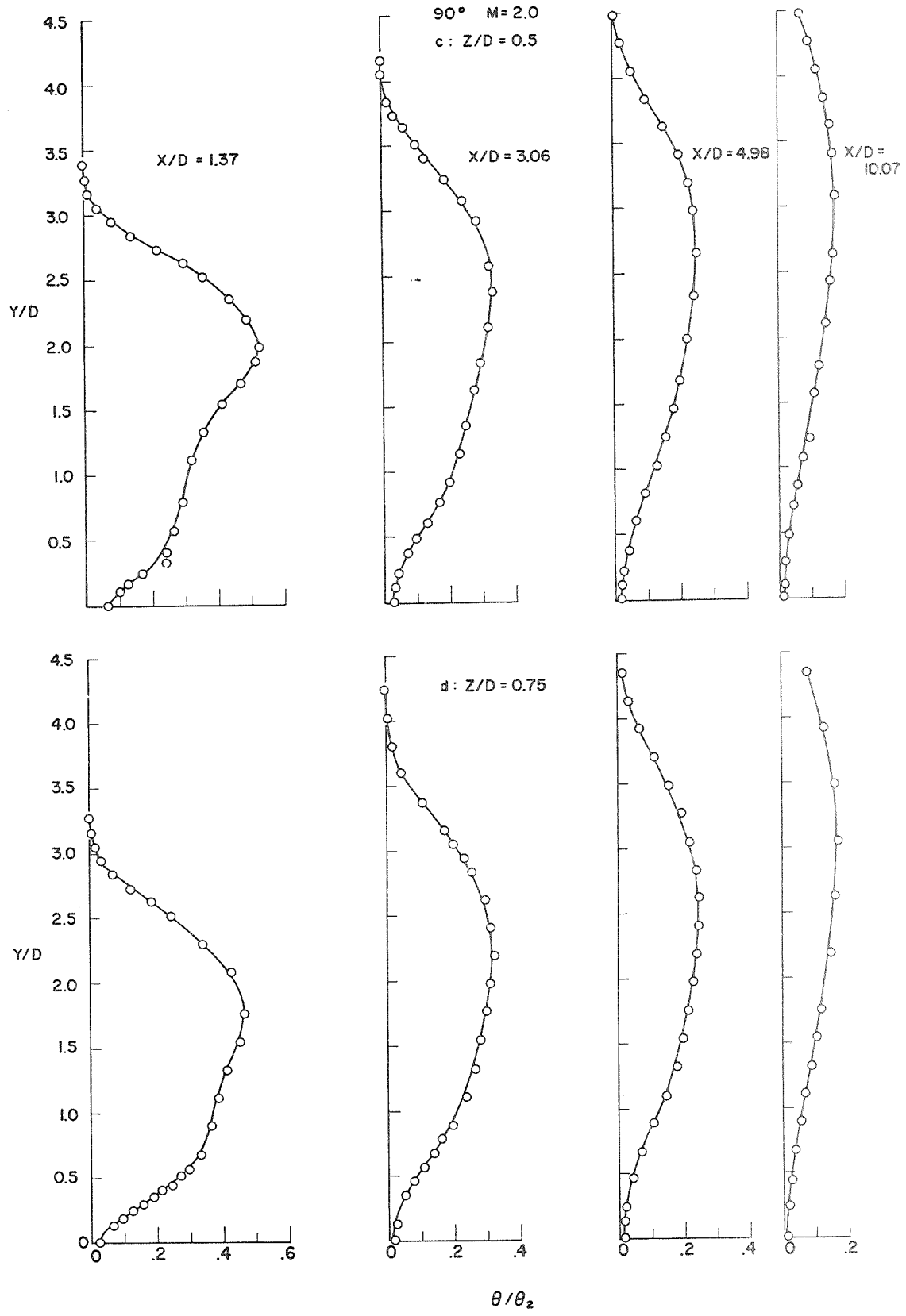

Figure A7b

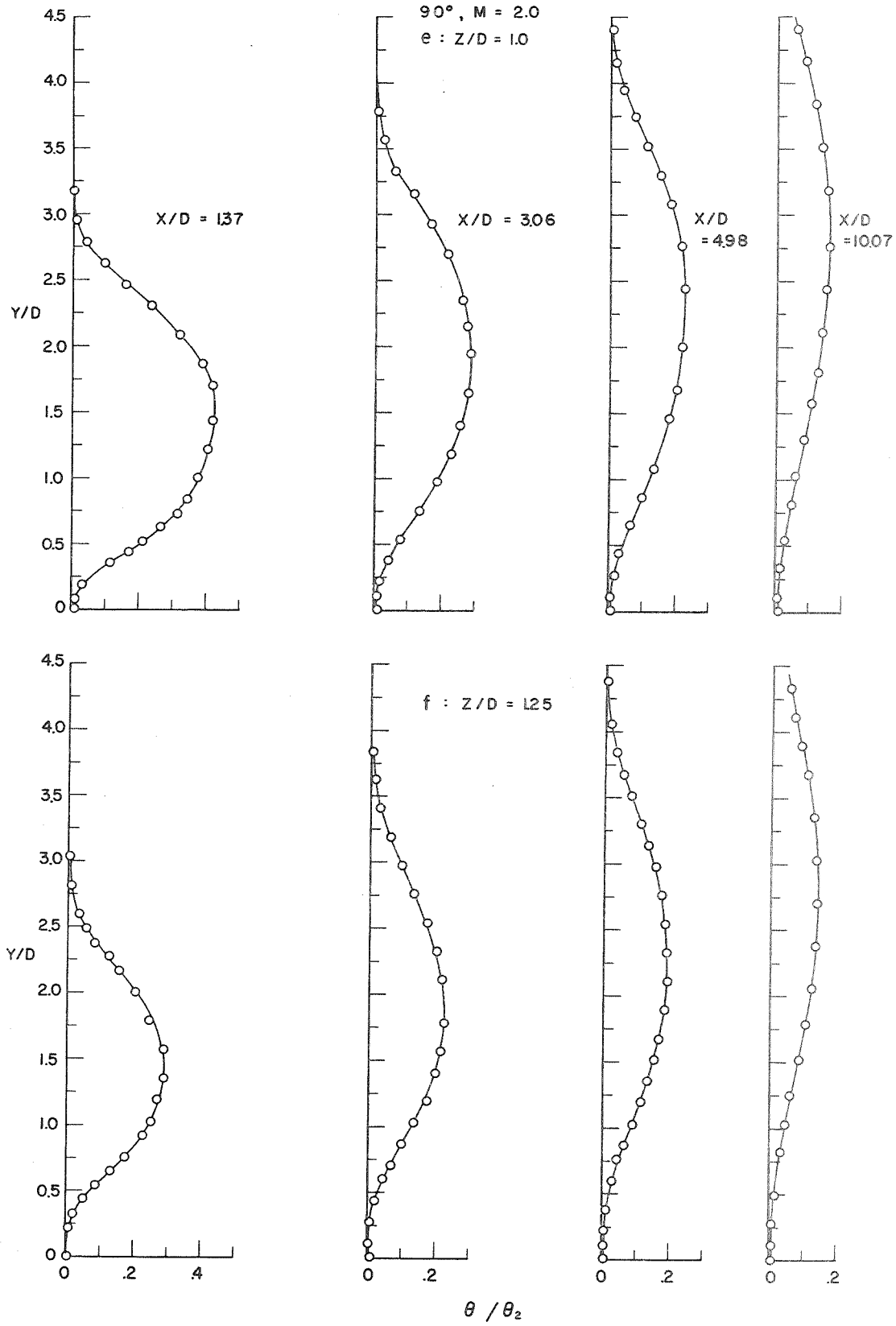

Figure A7c

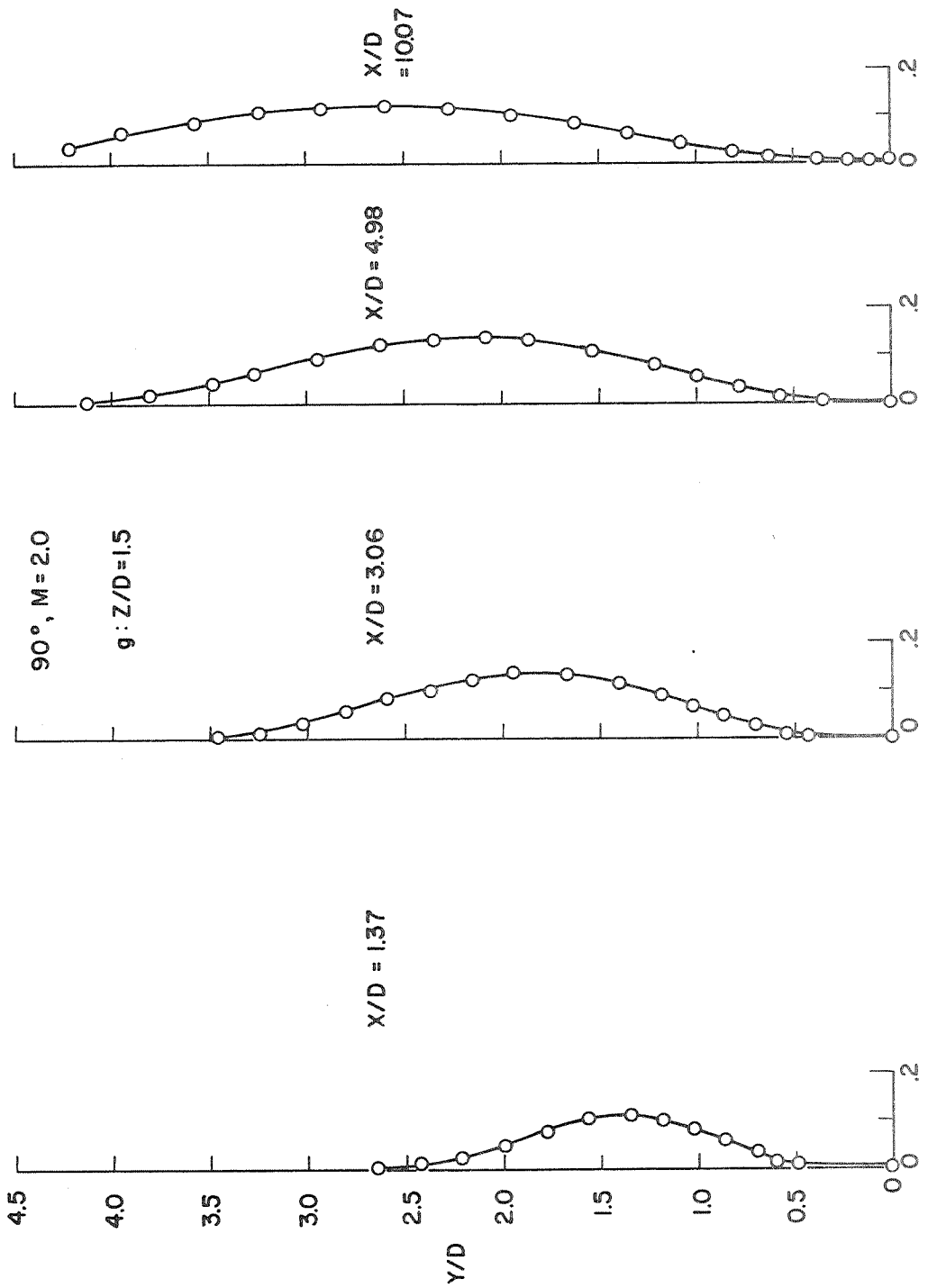
90°, M=2.0
g: Z/D=1.5
X/D = 1.37
X/D=3.06
X/D=4.98
X/D =10.07
Y/D
θ/θ₂
0
.2
0.5
1.0
1.5
2.0
2.5
3.0
3.5
4.0
4.5

Figure A7d

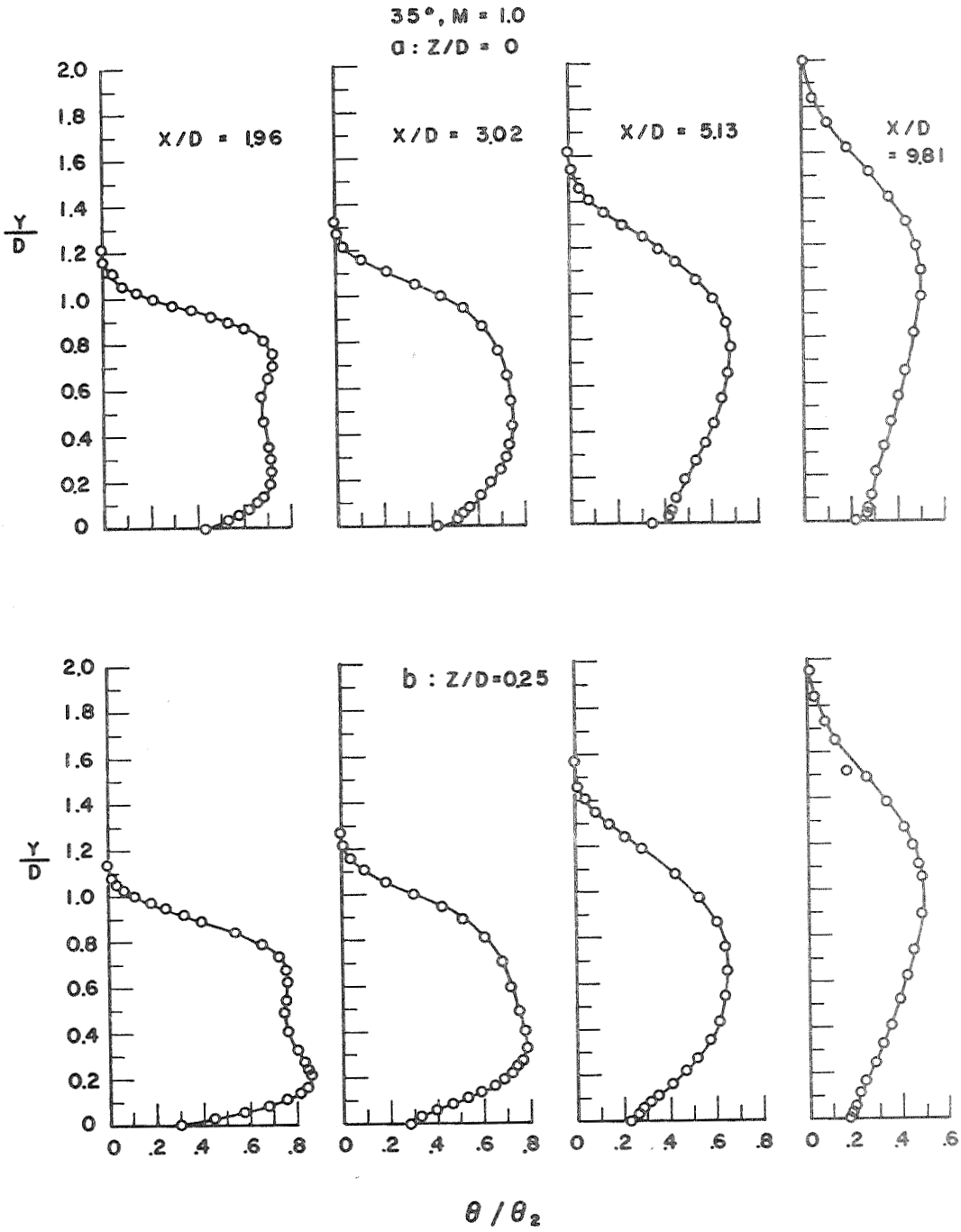

Figure A8a Temperature profiles for 35^{o} injection angle, M=1.0.

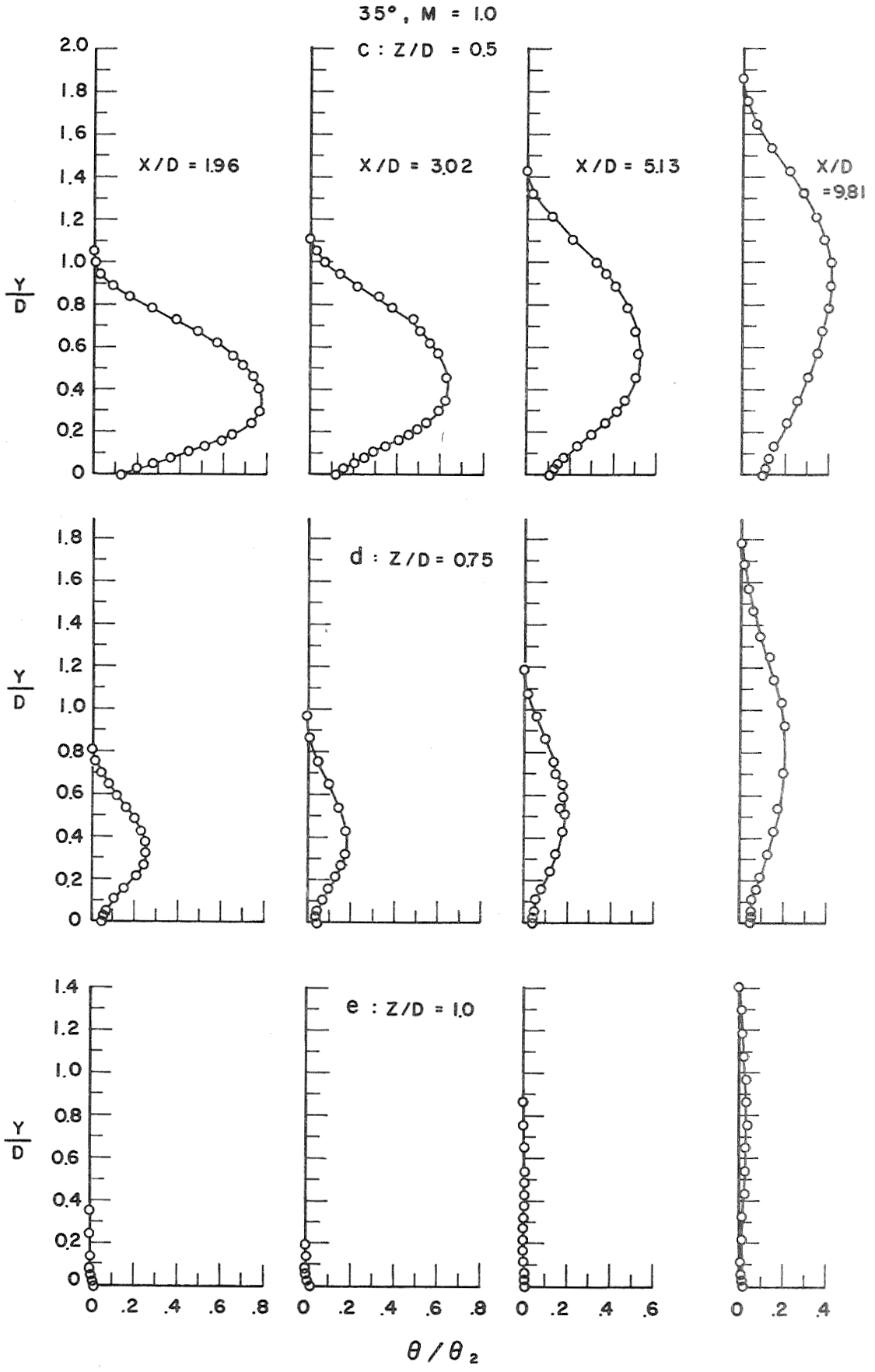

Figure A8b

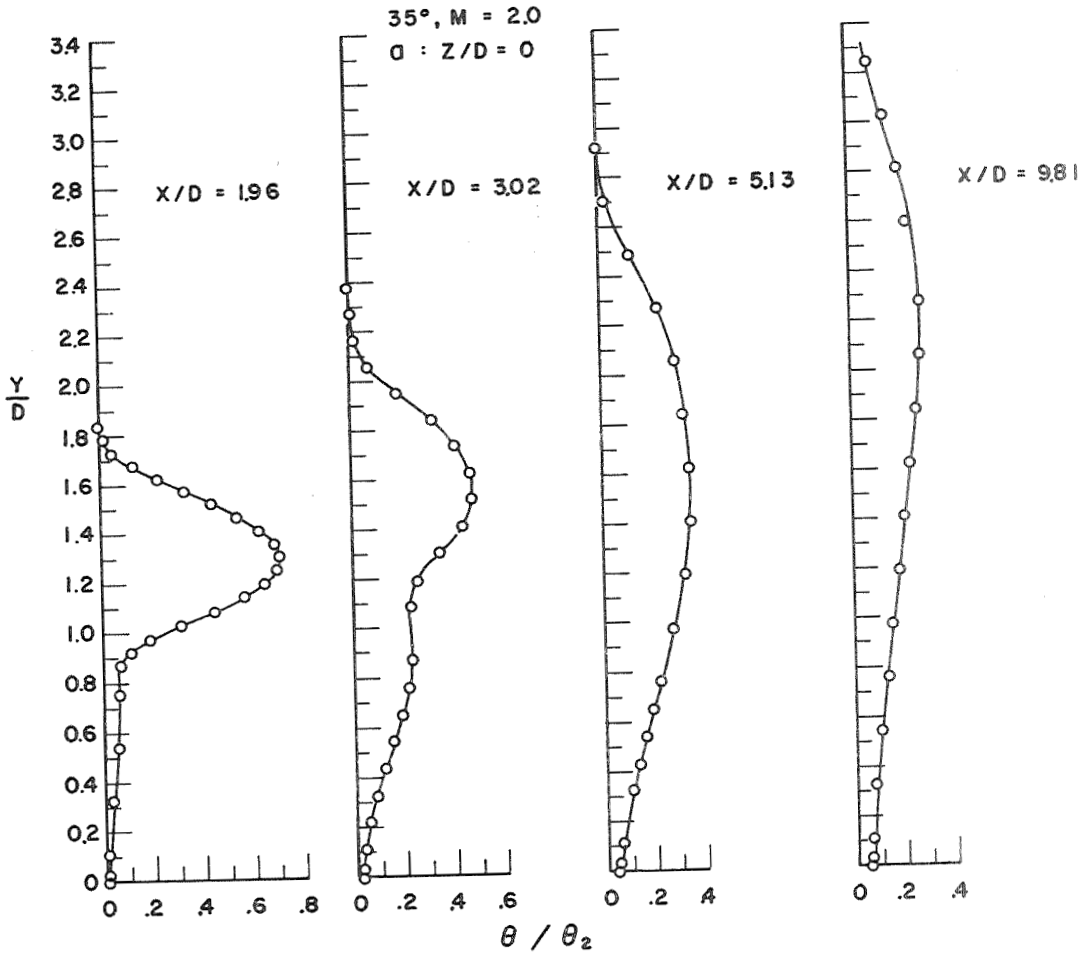

Figure A9a Temperature profiles for 35° injection angle, M=2.0.

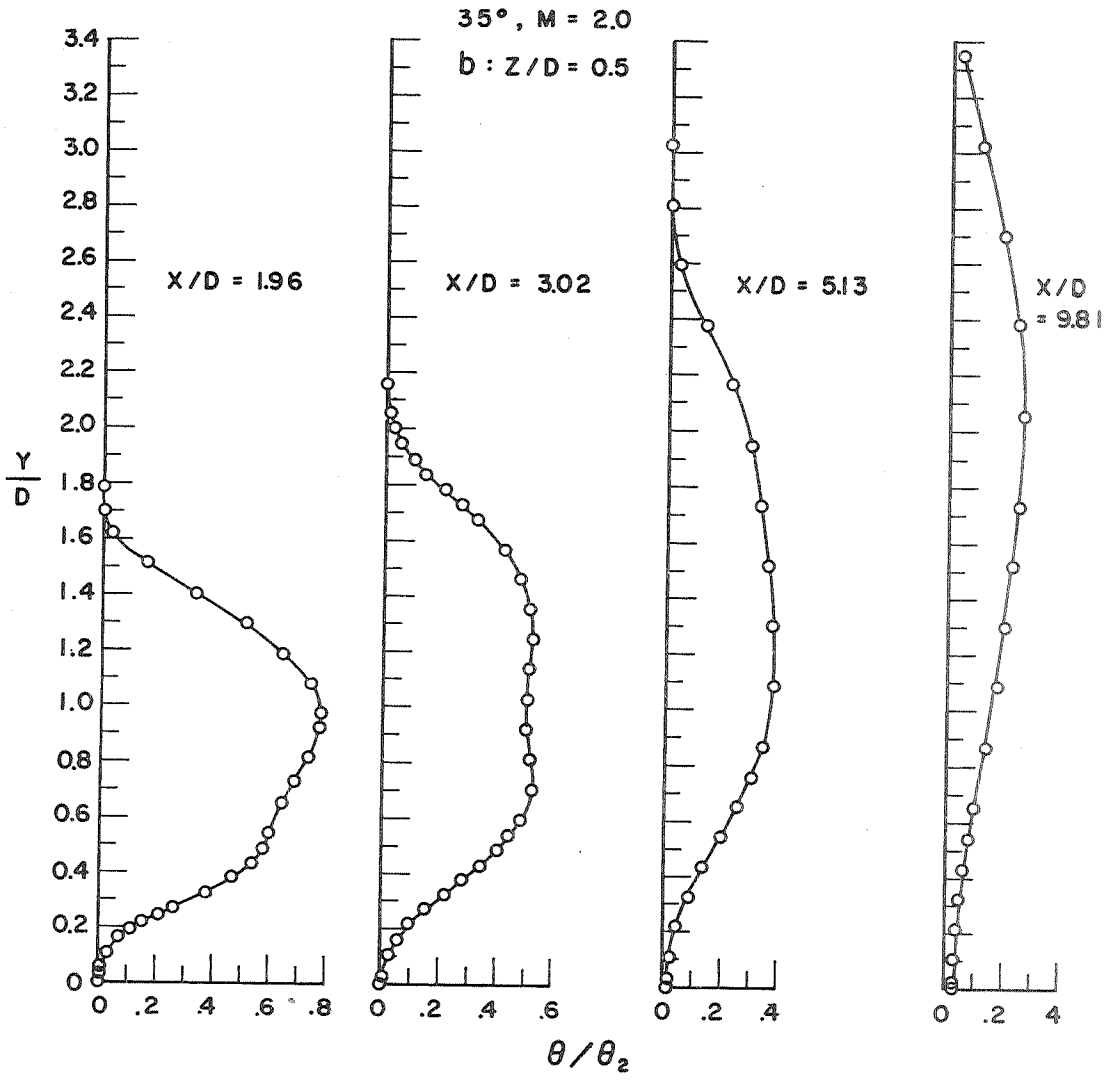
35°, M = 2.0
b : Z/D = 0.5
X/D = 1.96
X/D = 3.02
X/D = 5.13
X/D = 9.81
Y/D
θ/θ₂
3.4
3.2
3.0
2.8
2.6
2.4
2.2
2.0
1.8
1.6
1.4
1.2
1.0
0.8
0.6
0.4
0.2
0
0 .2 .4 .6 .8
0 .2 .4 .6
0 .2 .4
0 .2 4

Figure A9b

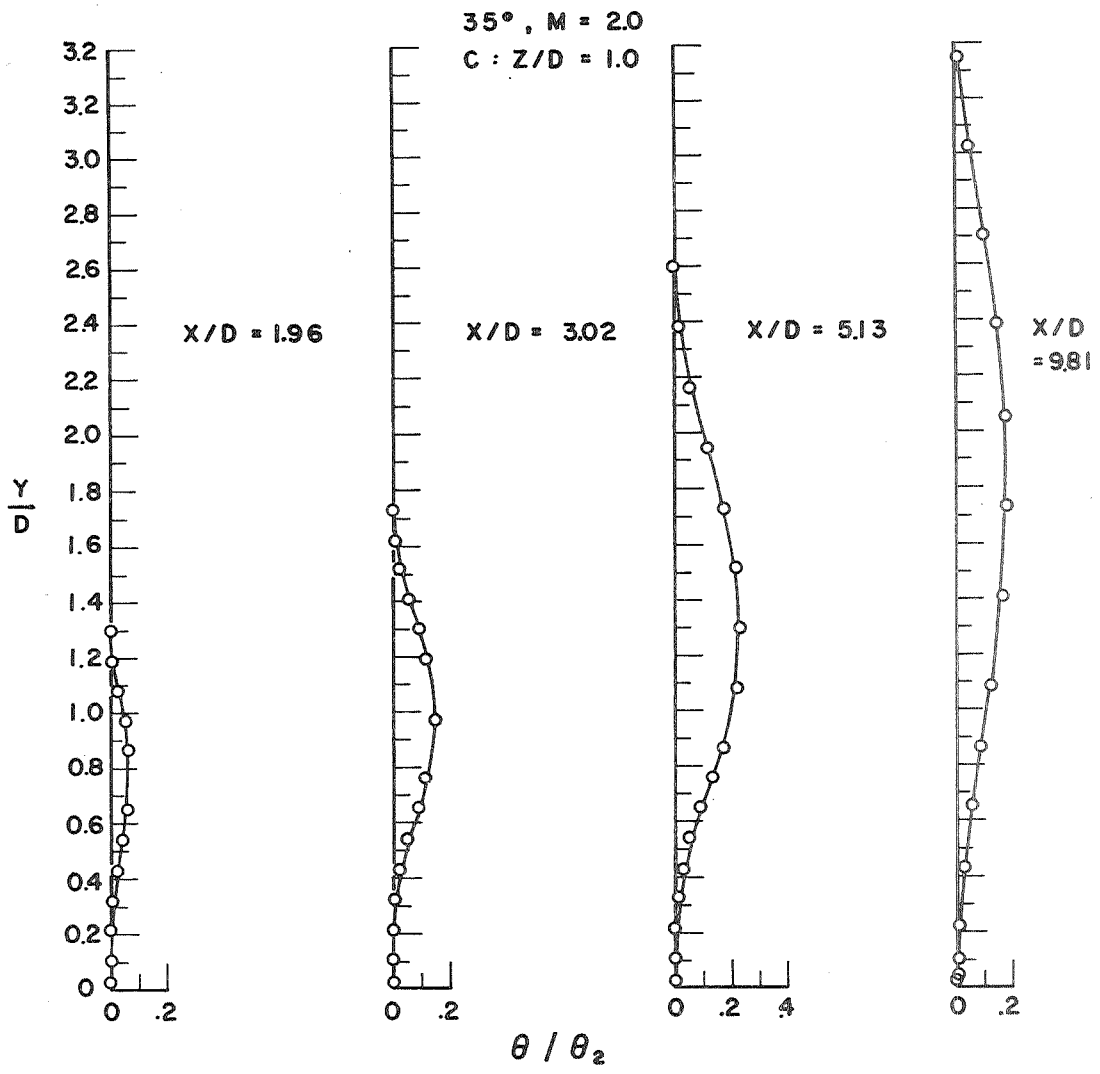

Figure A9c

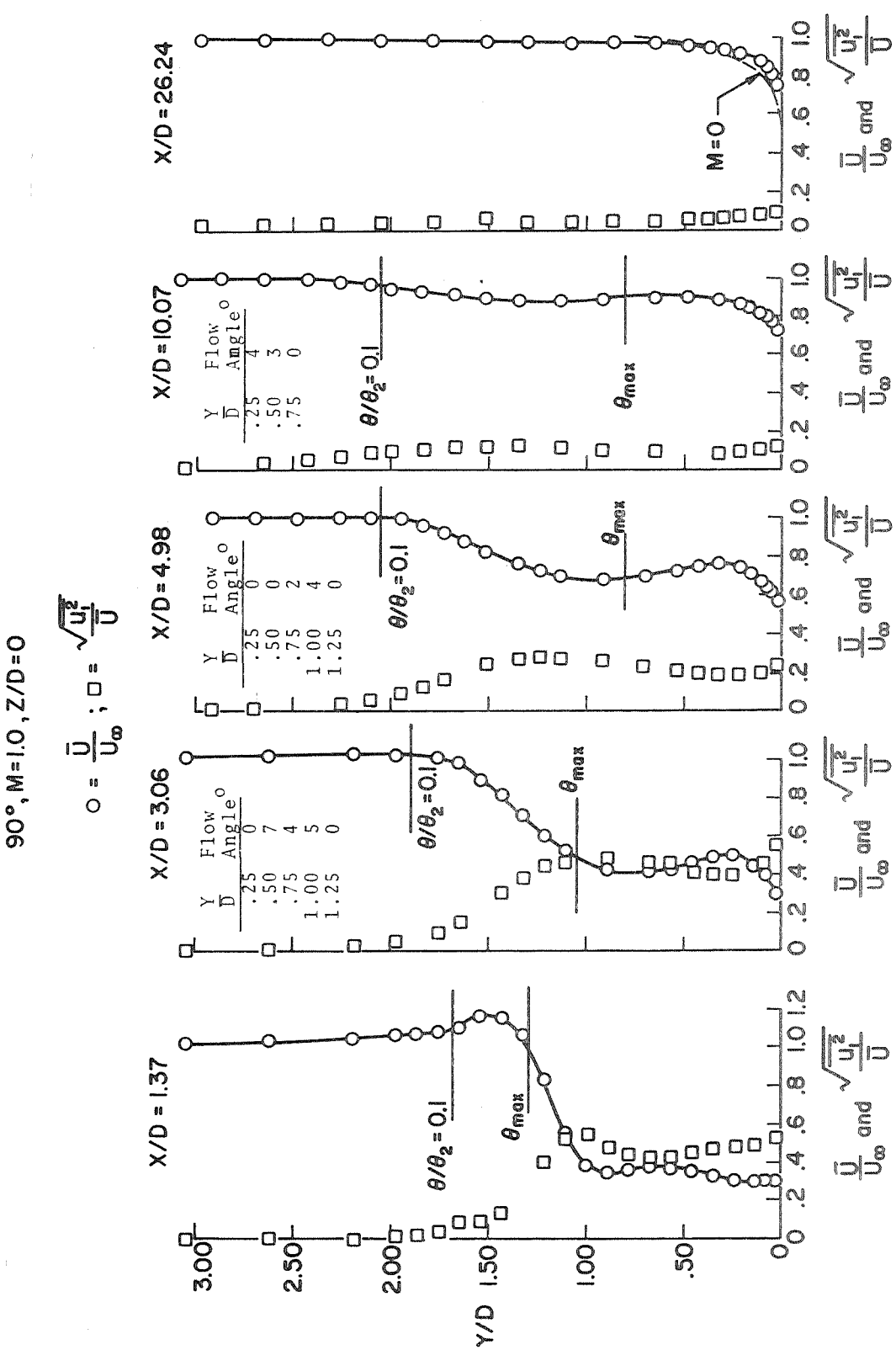

Figure A10a Velocity and turbulence intensity profiles for 90° injection angle, Z/D=0, M=1.0.

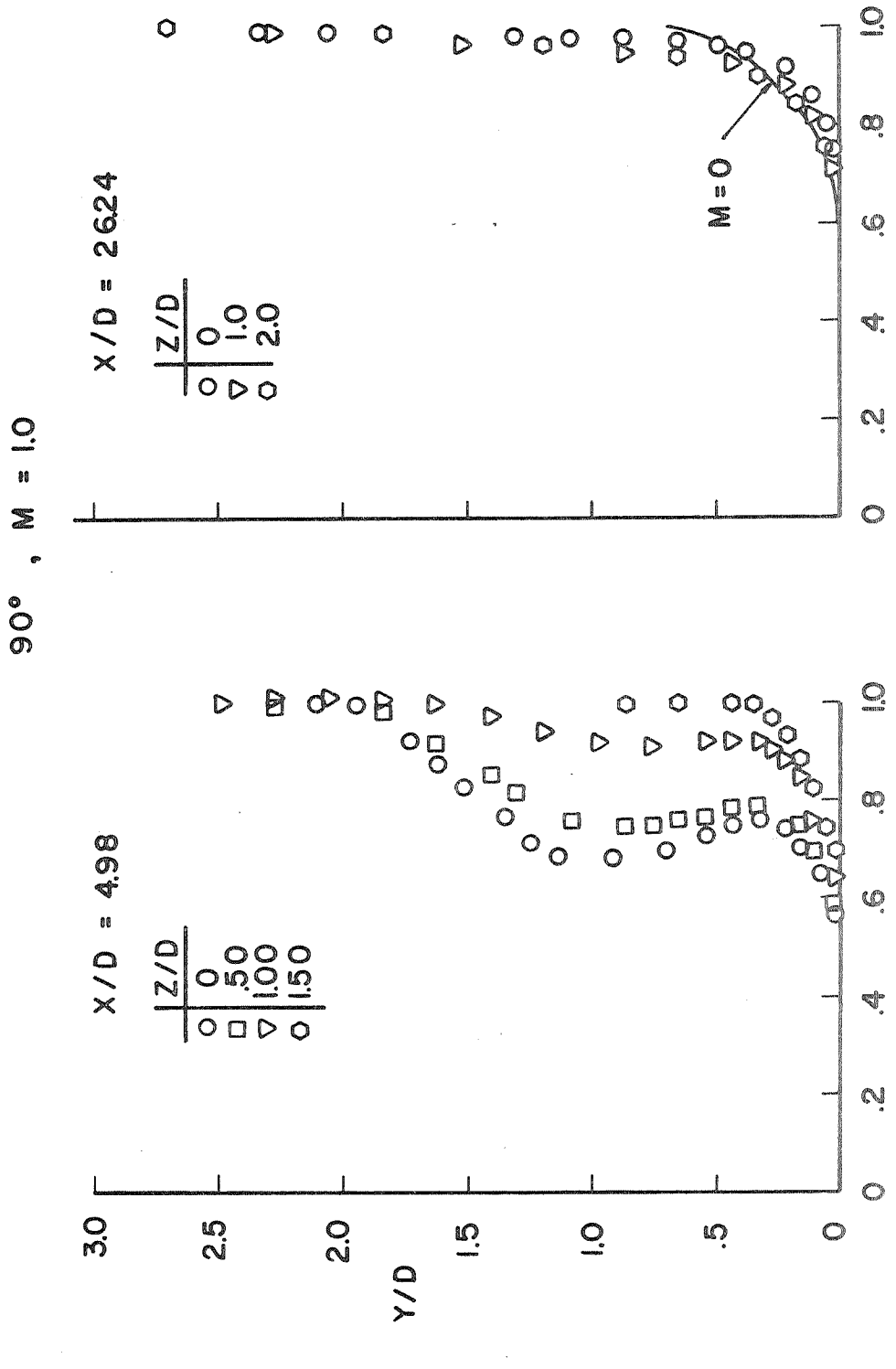
90° , M = 1.0
X/D = 4.98
Z/D
0
.50
1.00
1.50
X/D = 26.24
Z/D
0
1.0
2.0
M = 0
Y/D
3.0
2.5
2.0
1.5
1.0
.5
0
0
.2
.4
.6
.8
1.0
$\overline{U}/U_\infty$

Figure A10b

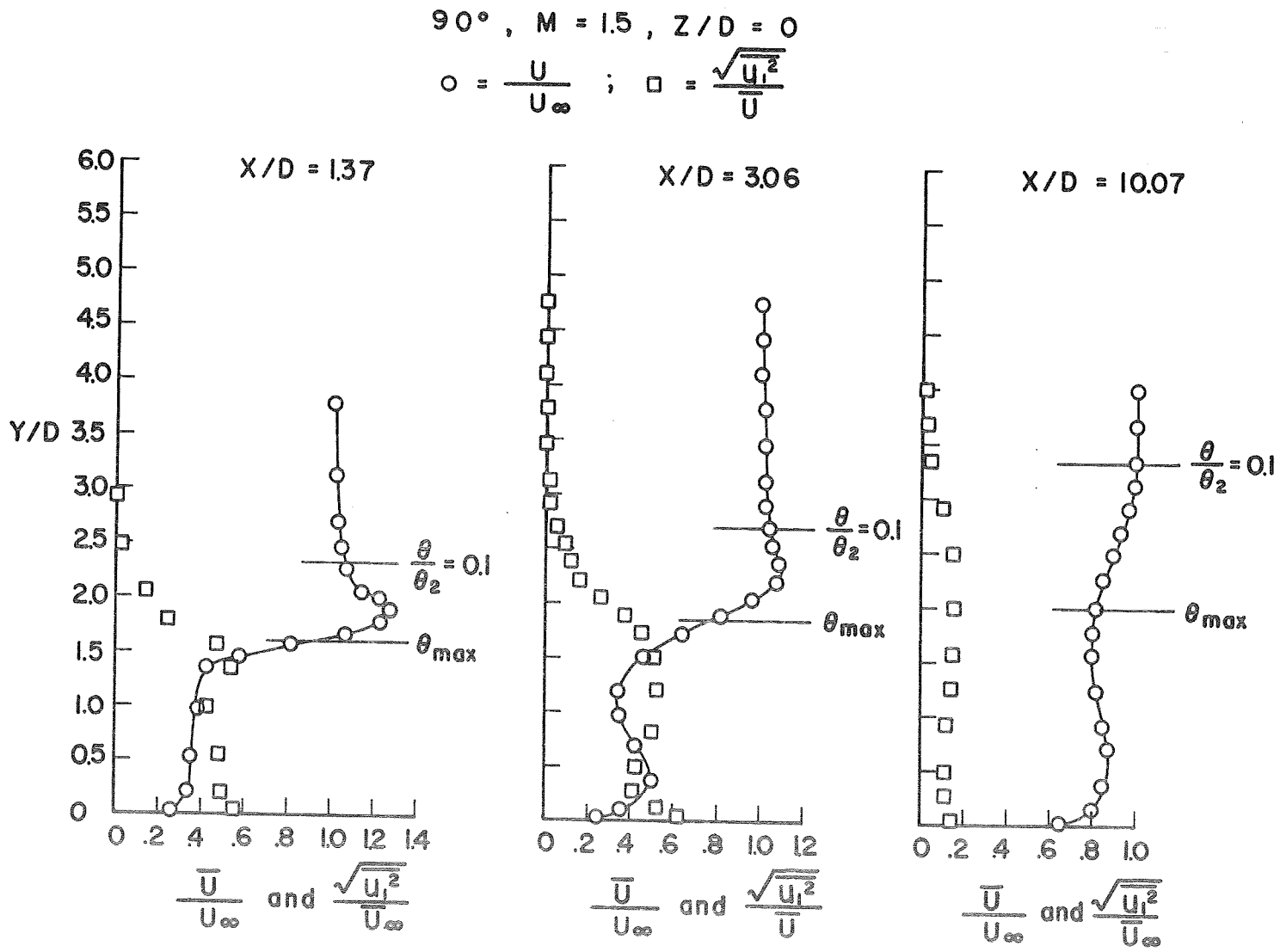

Figure A11 Velocity and turbulence intensity profiles for 90° injection angle, Z/D=0, M=1.5.

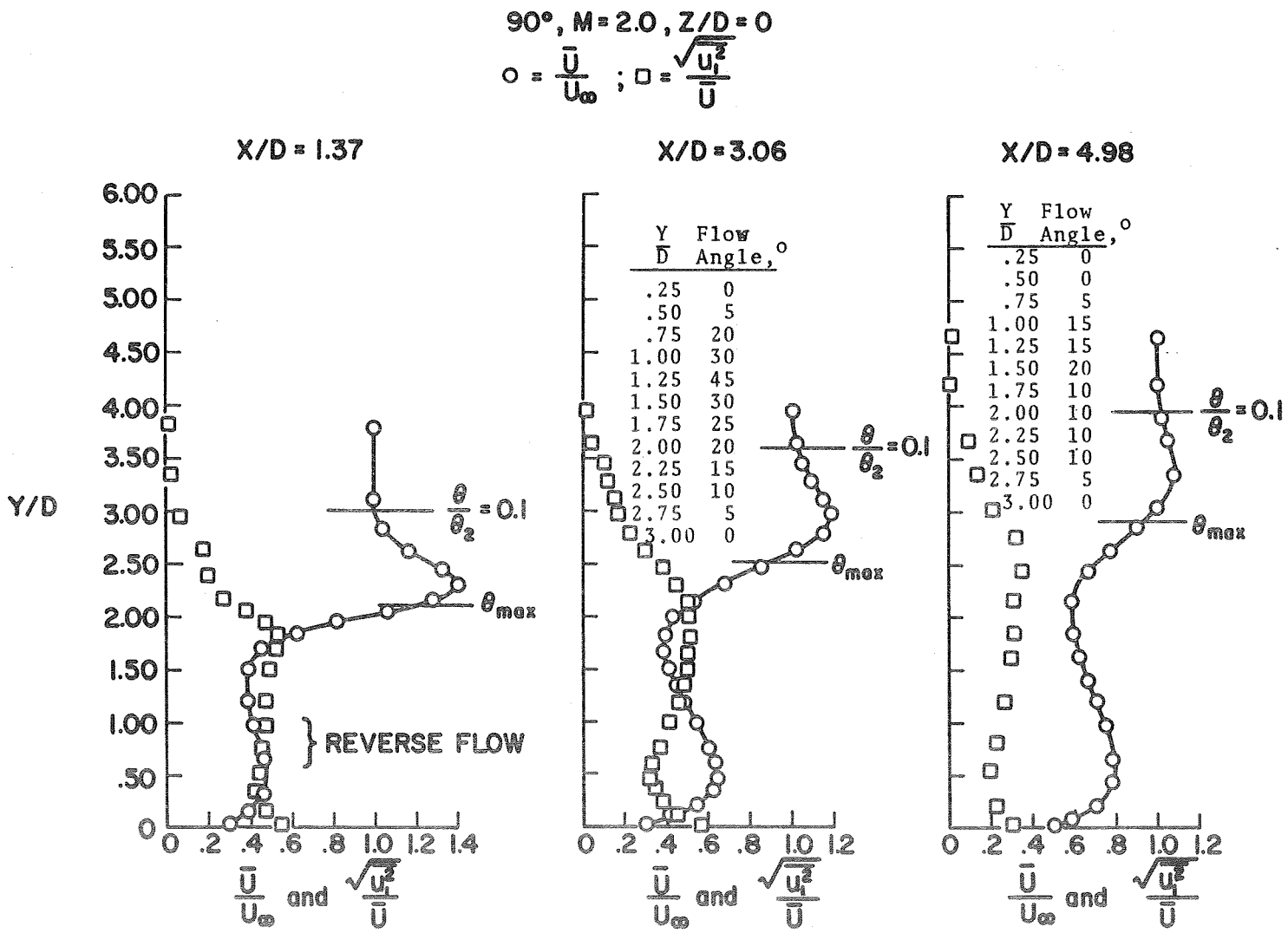

Figure A12a Velocity and turbulence intensity profiles for 90° injection angle, Z/D=0, M=2.0.

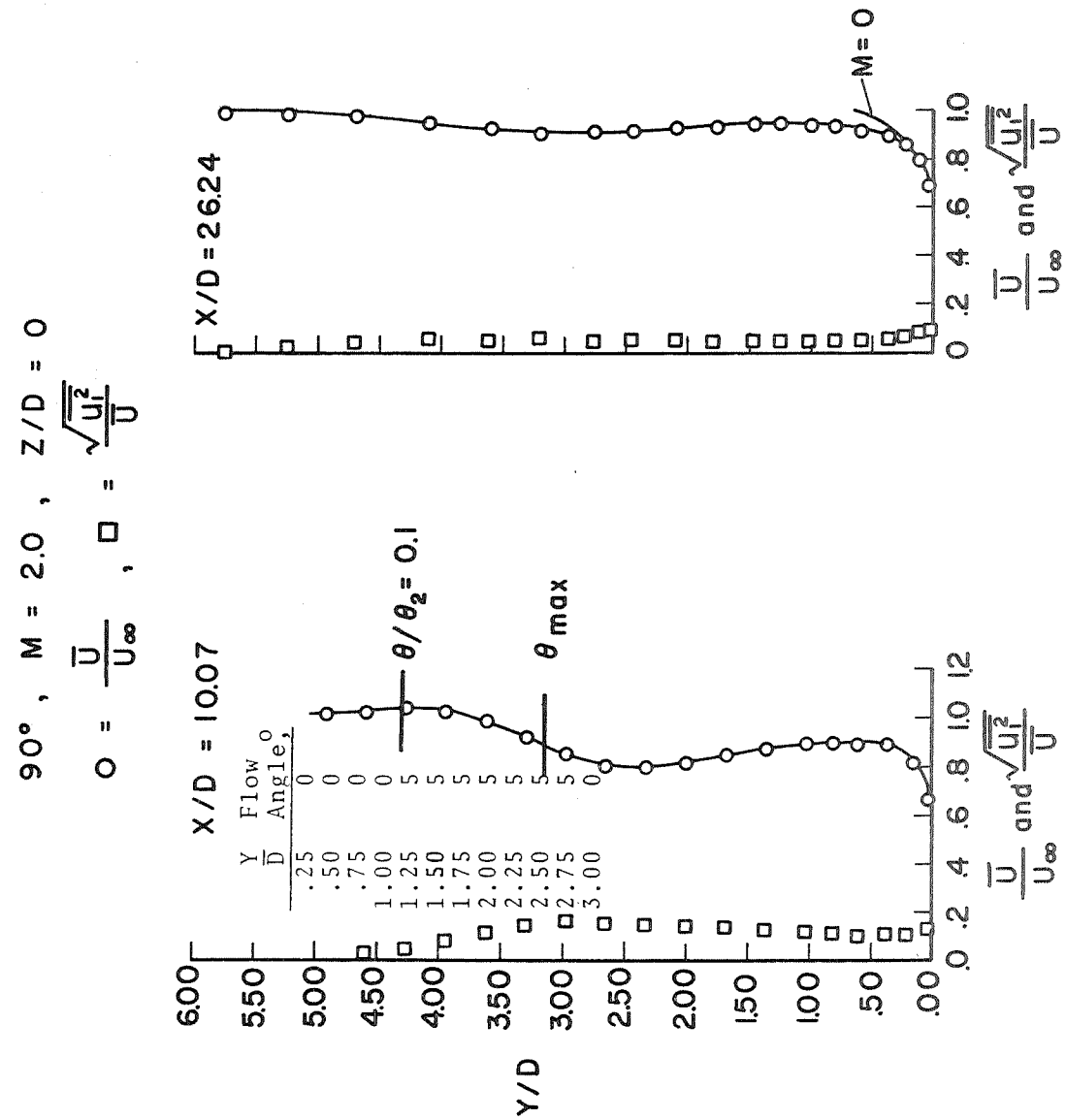
90°, M = 2.0, Z/D = 0
O = U/U∞, □ = √(u_i²)/U
X/D = 10.07
Y/D
Y/D Flow Angle, °
.25 0
.50 0
.75 0
1.00 0
1.25 5
1.50 5
1.75 5
2.00 5
2.25 5
2.50 5
2.75 5
3.00 0
θ/θ2 = 0.1
θ max
U/U∞ and √(u_i²)/U
X/D = 26.24
M = 0
U/U∞ and √(u_i²)/U

Figure A12b

NAS3-7904
SUMMARY REPORT
DISTRIBUTION LIST

ADDRESSEE		Mail Stop	NUMBER OF COPIES
1.	NASA Lewis Research Center 21000 Brookpark Road Cleveland, Ohio 44135		
	Attention: Aeronautics Procurement Section	77-3	1
	Reports Control Office	5-5	1
	Technology Utilization Office	3-19	1
	Library	60-3	2
	Fluid System Components Div.	5-3	1
	W. L. Stewart	77-2	1
	J. Howard Childs	60-4	1
	J. B. Esgar	60-4	1
	F. S. Stepka	60-6	10
	R. O. Hickel	60-6	1
	H. Ellerbrock	60-4	6
	J. Livingood	60-6	1
	E. L. Warren	60-6	1
	J. S. Clark	60-6	1
2.	NASA Scientific & Technical Information Facility P.O. Box 33 College Park, Maryland 20740 Attention: NASA Representative RQT-2448		6
3.	FAA Headquarters 800 Independence Avenue, S.W. Washington, D.C. 20546 Attention: Robert Pines		1
4.	NASA Headquarters Washington, D.C. 20546 Attention: N. F. Rekos (RAP)		1
5.	Department of the Army U.S. Army Aviation Material Laboratory Fort Eustis, Va. 23604 Attention: John White		1
6.	Headquarters Wright-Patterson AFB, Ohio 45433 Attention: Kenneth Hopkins (AFAPL/APTC)		2

7. Air Force Office of Scientific Research
Propulsion Research Division
USAF Washington, D.C. 20025 — 1

8. Defense Documentation Center (DDC)
Cameron Station
5010 Duke Street
Alexandria, Virginia 22314 — 1

9. NASA-Langley Research Center
Langley Station
Technical Library
Hampton, Virginia 23365
Attention: Mark R. Nichols — 1
John V. Becker — 1

10. United Aircraft Corporation
Pratt & Whitney Aircraft Division
Florida Research & Development Center
P.O. Box 2691
West Palm Beach, Florida 33402
Attention: R. A. Schmidtke — 1

11. United Aircraft Corporation
Pratt & Whitney Aircraft Division
400 Main Street
East Hartford, Connecticut 06108
Attention: C. Andreini — 2
Library — 1
M. Suo — 1

12. United Aircraft Research
East Hartford, Connecticut
Attention: Library — 1

13. Allison Division of GMC
Department 8894, Plant 8
P.O. Box 894
Indianapolis, Indiana 46206
Attention: J. N. Barney — 1
C. E. Holbrook — 1
Library — 1

14. Northern Research & Engineering Corporation
219 Vassar Street
Cambridge, Massachusetts
Attention: K. Ginwala — 1

15. General Electric Company
Flight Propulsion Division
Cincinnati, Ohio 45125
Attention: J. W. McBride N-44 1
F. Burggraf H-32 1
S. N. Suciu H-32 1
Technical Information Center N-32 1

16. General Electric Company
1000 Western Avenue
West Lynn, Massachusetts 01905
Attention: Dr. C. W. Smith--Library Bldg. 2-40M 1

17. Curtiss-Wright Corporation
Wright Aeronautical Division
Wood-Ridge, New Jersey 07075
Attention: S. Lombardo 1

18. Air Research Manufacturing Company
402 South 36th Street
Phoenix, Arizona 85034
Attention: Robert O. Bullock 1

19. Air Research Manufacturing Company
9851 Sepulveda Boulevard
Los Angeles, California 90009
Attention: Dr. P. J. Berenson 1

20. AVCO Corporation
Lycoming Division
350 South Main Street
Stratford, Connecticut 06497
Attention: Claus W. Bolton 1
Charles Kuintzle 1

21. Continental Aviation & Engineering Corporation
12700 Kercheval
Detroit, Michigan 48215
Attention: Eli H. Benstein 1
Howard C. Walch 1

22. International Harvester Company
Solar Division - 2200 Pacific Highway
San Diego, California 92112
Attention: P. A. Pitt 1
Mrs. L. Walper 1

23. George Derderian AIR 53662B
Department of Navy
Bureau of Navy
Washington, D.C. 20360 — 1

24. The Boeing Company
Commercial Airplane Division
P.O. Box 3991
Seattle, Washington 98124
Attention: C. J. Schott — 80-66 — 1

25. Aerojet-General Corporation
Sacramento, California 95809
Attention: M. S. Nylin — 1
Library — 1
William Heath — 1

26. Newark College of Engineering
323 High Street
Newark, New Jersey 07102
Attention: Dr. Peter Hrycak — 1

27. Department of Mechanical Engineering
Arizona State University
Tempe, Arizona
Attention: Dr. D. E. Metzger — 1

28. Dr. W. Kays
Stanford University
Stanford, California — 1